

# CONSISTENCY MODELS MADE EASY

Zhengyang Geng<sup>1</sup>   Ashwini Pople<sup>1</sup>   William Luo<sup>2</sup>   Justin Lin<sup>1</sup>   J. Zico Kolter<sup>1</sup>

<sup>1</sup>CMU   <sup>2</sup>Westlake University

## ABSTRACT

Consistency models (CMs) offer faster sampling than traditional diffusion models, but their training is resource-intensive. For example, as of 2024, training a state-of-the-art CM on CIFAR-10 takes one week on 8 GPUs. In this work, we propose an effective scheme for training CMs that largely improves the efficiency of building such models. Specifically, by expressing CM trajectories via a particular differential equation, we argue that diffusion models can be viewed as a special case of CMs. We can thus fine-tune a consistency model starting from a pretrained diffusion model and progressively approximate the full consistency condition to stronger degrees over the training process. Our resulting method, which we term Easy Consistency Tuning (ECT), achieves vastly reduced training times while improving upon the quality of previous methods: for example, ECT achieves a 2-step FID of 2.73 on CIFAR10 within 1 hour on a single A100 GPU, matching Consistency Distillation trained for hundreds of GPU hours. Owing to this computational efficiency, we investigate the scaling laws of CMs under ECT, showing that they obey the classic power law scaling, hinting at their ability to improve efficiency and performance at larger scales. Our [code](#) is publicly available, making CMs more accessible to the broader community.

## 1 INTRODUCTION

Diffusion Models (DMs) (Ho et al., 2020; Song et al., 2021a), or Score-based Generative Models (SGMs) (Song et al., 2020; 2021b), have vastly changed the landscape of visual content generation with applications in images (Rombach et al., 2021; Saharia et al., 2022; Ho et al., 2022a; Dhariwal and Nichol, 2021; Hatamizadeh et al., 2023; Ramesh et al., 2021), videos (Brooks et al., 2024; Blattmann et al., 2023; Bar-Tal et al., 2024; Ho et al., 2022b; Gupta et al., 2023), and 3D objects (Poole et al., 2022; Wang et al., 2024a; Lee et al., 2024; Chen et al., 2024; Babu et al., 2023). DMs progressively transform a data distribution to a known prior distribution (e.g. Gaussian noise) according to a stochastic differential equation (SDE) (Song et al., 2021b) and train a model to denoise noisy observations. Samples can be generated via a reverse-time SDE that starts from noise and uses the trained model to progressively denoise it. However, sampling from a DM naively requires hundreds to thousands of model evaluations due to the curvature of the diffusion sampling trajectory (Karras et al., 2022), making the entire generative process slow. Many approaches have been proposed to address this issue, including training-based techniques such as distillation (Luhman and Luhman, 2021; Salimans and Ho, 2022; Luo et al., 2024; Gu et al., 2023; Sauer et al., 2023; Geng et al., 2024; Yin et al., 2023; Nguyen and Tran, 2023), adaptive compute architectures for the backbone model (Moon et al., 2023; Tang et al., 2023), as well as training-free methods such as fast samplers (Kong and Ping, 2021; Lu et al., 2022a; Zhang and Chen, 2022; Zhou et al., 2023; Xue et al., 2024) or interleaving small and large backbone models during sampling (Pan et al., 2024). However, the speedup achieved by these sampling techniques usually comes at the expense of the quality of generated samples.

Consistency Models (CMs) (Song et al., 2023) are a new family of generative models, closely related to diffusion models, that have demonstrated promising results as faster generative models. These models learn a mapping between noise and data, and all the points of the sampling trajectory map to the same initial data point. Owing to this condition, consistency models are capable of generating high-quality samples in 1-2 model evaluations. The best such models so far, built using improved Consistency Training (iCT) (Song and Dhariwal, 2023), have pushed the quality of images generated by 1-step CMs trained from scratch to a level comparable with SoTA DMs using thousands of steps for

sampling. Unfortunately, CMs remain time-consuming and practically challenging to train: the best practice takes many times longer than similar-quality DMs while involving complex hyperparameter choices in the training process. In total, this has substantially limited the uptake of CMs within the community.

In this work, we introduce a differential perspective on consistency models, leading to the formulation of the differential consistency condition in continuous time. This insight reveals the link between diffusion models and consistency models, viewing DMs as a special case of CMs with loose discretization. This observation motivates us to smoothly interpolate from DM to CM by progressively tightening the consistency condition, bootstrapping pretrained DMs to 1-step CMs w/o using extra frozen teachers. We term this strategy as *Easy Consistency Tuning (ECT)*, which includes diffusion pretraining as a special stage of the continuous time training schedule.

ECT significantly improves both training efficiency and performance. On ImageNet  $64 \times 64$  (Deng et al., 2009), ECT achieves superior 1-step and 2-step sample quality compared to the prior art. Similarly, on CIFAR-10 (Krizhevsky, 2009) 2-step sample quality of ECT surpasses previous methods. The total cost of the pretraining and tuning scheme requires only  $1/4 \sim 1/3$  of the computational resources (FLOPs) used by the current state-of-the-art method, iCT (Song and Dhariwal, 2023), while the tuning stage can be remarkably lightweight, typically accounting for 10% or less of the overall cost and further benefiting from scaling.

Leveraging ECT’s computational efficiency, we conduct the first study into the scaling behaviors of CMs, revealing the classic power law scaling for model size, FLOPs, and training compute. The scaling also suggests a sweet spot of using smaller few-step CMs over larger 1-step CMs in certain scenarios. This computational efficiency enables us to explore the design space of CMs by using the tuning stage as a proxy. Notably, tuning findings, such as weighting functions, can improve the pretraining stage and, in turn, enhance the overall pretraining + tuning pipeline for CMs.

In short, we summarize our contributions as follows:

- We develop Easy Consistency Tuning (ECT), a pretraining + tuning scheme for training CMs in continuous time, demonstrating significant efficiency and performance gains compared to the current best practices for training CMs.
- We investigate CMs’ scaling behaviors for the first time and reveal the classic power law.
- We explore the design space of CMs through ECT, introducing the continuous-time schedule and better weighting functions for CMs.

## 2 PRELIMINARIES

**Diffusion Models.** Let  $p_{\text{data}}(\mathbf{x}_0)$  denote the data distribution. Diffusion models (DMs) perturb this distribution by adding monotonically increasing i.i.d. Gaussian noise with standard deviation  $\sigma(t)$  from  $t = 0$  to  $T$  such that  $p_t(\mathbf{x}_t|\mathbf{x}_0) = \mathcal{N}(\mathbf{x}_0, \sigma^2(t)\mathbf{I})$ , and  $\sigma(t)$  is chosen such that  $\sigma(0) = \sigma_{\min}$  and  $\sigma(T) = \sigma_{\max}$ . This process is described by the following SDE (Song et al., 2021b)

$$d\mathbf{x}_t = \mathbf{f}(\mathbf{x}_t, t)dt + g(t)d\mathbf{w}_t, \quad (1)$$

where  $\mathbf{w}$  is the standard Wiener process,  $\mathbf{f}(\cdot, t) : \mathbb{R}^d \rightarrow \mathbb{R}^d$  is the drift coefficient, and  $g(\cdot) : \mathbb{R} \rightarrow \mathbb{R}$  is the diffusion coefficient. Samples can be generated by solving the reverse-time SDE starting from  $t = T$  to 0 and sampling  $\mathbf{x}_T \sim \mathcal{N}(0, \sigma_{\max}^2\mathbf{I})$ . (Song et al., 2021b) show that this SDE has a corresponding ODE, called the probability flow ODE (PF-ODE), whose trajectories share the same marginal probability densities as the SDE. We follow the notation in (Karras et al., 2022) to describe the ODE as

$$d\mathbf{x}_t = -\dot{\sigma}(t)\sigma(t)\nabla_{\mathbf{x}_t} \log p_t(\mathbf{x}_t)dt, \quad (2)$$

where  $\nabla_{\mathbf{x}_t} \log p_t(\mathbf{x}_t)$  denotes the score function. Prior works (Karras et al., 2022; Song et al., 2023) set  $\sigma(t) = t$  which yields

$$\frac{d\mathbf{x}_t}{dt} = -t\nabla_{\mathbf{x}_t} \log p_t(\mathbf{x}_t) = \frac{(\mathbf{x}_t - f(\mathbf{x}_t, t))}{t}, \quad (3)$$

where  $f(\mathbf{x}_t, t)$  denotes a denoising function that predicts clean image  $\mathbf{x}_0$  given noisy image  $\mathbf{x}_t$ . We will follow this parametrization in the rest of this paper. Note that time is same as noise level with this parametrization, and we will use these two terms interchangeably.

**Consistency Models.** CMs are built upon the PF-ODE in Eq. (3), which establishes a bijective mapping between data distribution and noise distribution. CMs learn a *consistency function*  $f(\mathbf{x}_t, t)$  that maps the noisy image  $\mathbf{x}_t$  back to the clean image  $\mathbf{x}_0$

$$f(\mathbf{x}_t, t) = \mathbf{x}_0. \quad (4)$$

Note that the consistency function needs to satisfy the boundary condition at  $t = 0$ . Prior works (Karras et al., 2022; Song et al., 2023; Song and Dhariwal, 2023) impose this boundary condition by parametrizing the CM as

$$f_\theta(\mathbf{x}_t, t) = c_{\text{skip}}(t) \mathbf{x}_t + c_{\text{out}}(t) F_\theta(\mathbf{x}_t, t), \quad (5)$$

where  $\theta$  is the model parameter,  $F_\theta$  is the network to train, and  $c_{\text{skip}}(t)$  and  $c_{\text{out}}(t)$  are time-dependent scaling factors such that  $c_{\text{skip}}(0) = 1$ ,  $c_{\text{out}}(0) = 0$ . This parameterization guarantees the boundary condition by design. We discuss specific choices of  $c_{\text{skip}}(t)$  and  $c_{\text{out}}(t)$  in Appendix D.

During training, CMs first discretize the PF-ODE into  $N - 1$  subintervals with boundaries given by  $t_{\min} = t_1 < t_2 < \dots < t_N = T$ . The model is trained on the following CM loss, which minimizes a metric between adjacent points on the sampling trajectory

$$\arg \min_{\theta} \mathbb{E} \left[ w(t_i) d(f_\theta(\mathbf{x}_{t_{i+1}}, t_{i+1}), f_{\theta-}(\tilde{\mathbf{x}}_{t_i}, t_i)) \right]. \quad (6)$$

Here,  $d(\cdot, \cdot)$  is a metric function, the  $f_\theta$  indicates a trainable neural network that is used to learn the consistency function,  $f_{\theta-}$  indicates an exponential moving average (EMA) of the past values of  $f_\theta$ , and  $\tilde{\mathbf{x}}_{t_i} = \mathbf{x}_{t_{i+1}} - (t_i - t_{i+1}) t_{i+1} \nabla_{\mathbf{x}_{t_{i+1}}} \log p_{t_{i+1}}(\mathbf{x}_{t_{i+1}})$ . Further, the discretization curriculum  $N$  should be adaptive and tuned during training to achieve good performance.

In the seminal work, (Song et al., 2023) use Learned Perceptual Similarity Score (LPIPS) (Zhang et al., 2018) as a metric function, set  $w(t_i) = 1$  for all  $t_i$ , and sample  $t_i$  according to the sampling scheduler by (Karras et al., 2022):  $t_i = \left( t_{\max}^{1/\rho} + \frac{i}{N-1} (t_{\min}^{1/\rho} - t_{\max}^{1/\rho}) \right)^\rho$  for  $i \in \mathcal{U}[1, N-1]$  and  $\rho = 0.7$ . Further, the score function  $\nabla_{\mathbf{x}_t} \log p(\mathbf{x}_t)$  can either be estimated from a pretrained diffusion model, which results in Consistency Distillation (CD), or can be estimated with an unbiased score estimator

$$\nabla_{\mathbf{x}_t} \log p(\mathbf{x}_t) = \mathbb{E} \left[ \nabla_{\mathbf{x}_t} \log p(\mathbf{x}_t | \mathbf{x}_0) \middle| \mathbf{x}_t \right] = \mathbb{E} \left[ -\frac{\mathbf{x}_t - \mathbf{x}_0}{t^2} \middle| \mathbf{x}_t \right], \quad (7)$$

which results in consistency training (CT).

The follow-up work, iCT (Song and Dhariwal, 2023), introduces several improvements that significantly improve training efficiency as well as the performance of CMs. First, the LPIPS metric, which introduces undesirable bias in generative modeling, is replaced with a Pseudo-Huber metric. Second, the network  $f_{\theta-}$  does not maintain an EMA of the past values of  $f_\theta$ . Third, iCT replaces the uniform weighting scheme  $w(t_i) = 1$  with  $w(t_i) = \frac{1}{t_{i+1} - t_i}$ . Further, the scaling factors of noise embeddings and dropout are carefully selected. Fourth, iCT introduces a complex discretization curriculum during training:

$$N(m) = \min(s_0 2^{\lfloor \frac{m}{M'} \rfloor}, s_1) + 1, \quad M' = \left\lceil \frac{M}{\log_2 \left[ \frac{s_1}{s_0} + 1 \right]} \right\rceil, \quad (8)$$

where  $m$  is the current number of iterations,  $M$  is the total number of iterations,  $\sigma_{\max}$  and  $\sigma_{\min}$  is the largest and smallest noise level for training,  $s_0 = 10$  and  $s_1 = 1280$  are hyperparameters. Finally, during training, iCT samples  $i \sim p(i) \propto \text{erf} \left( \frac{\log(t_{i+1}) - P_{\text{mean}}}{\sqrt{2} P_{\text{std}}} \right) - \text{erf} \left( \frac{\log(t_i) - P_{\text{mean}}}{\sqrt{2} P_{\text{std}}} \right)$  from a discrete Lognormal distribution, where  $P_{\text{mean}} = -1.1$  and  $P_{\text{std}} = 2.0$ .

### 3 PROBING CONSISTENCY MODELS

We will first introduce the differential consistency condition and the loss objective based on this condition. Next, we will analyze this loss objective and highlight the challenges of training CMs with it. Based on this analysis, we present our method, Easy Consistency Tuning (ECT). ECT is a simple, principled approach to efficiently train CMs to meet the (differential) consistency condition. The resulting CMs can generate high-quality samples in 1 or 2 sampling steps.

### 3.1 DIFFERENTIAL CONSISTENCY CONDITION

As stated in Sec. 2, CMs learn a *consistency function*  $f(\mathbf{x}_t, t)$  that maps the noisy image  $\mathbf{x}_t$  back to the clean image  $\mathbf{x}_0$ :  $f(\mathbf{x}_t, t) = \mathbf{x}_0$ . Instead, by taking the time derivative of both sides, given by the differential form

$$\frac{df}{dt} = \frac{d}{dt}\mathbf{x}_0 = 0. \quad (9)$$

However, the differential form  $\frac{df}{dt} = 0$  alone is not sufficient to guarantee that the model output will match the clean image, as there exist trivial solutions where the model maps all the inputs to a constant value, such as  $f(\mathbf{x}_t, t) \equiv 0$ . To eliminate these collapsed solutions, (Song et al., 2023; Song and Dhariwal, 2023) impose the boundary condition for  $f(\mathbf{x}_t, t) = \mathbf{x}_0$  via model parameterization:

$$f(\mathbf{x}_t, t) = \mathbf{x}_0 \Leftrightarrow \frac{df}{dt} = 0, f(\mathbf{x}_0, 0) = \mathbf{x}_0. \quad (10)$$

This boundary condition  $f(\mathbf{x}_0, 0) = \mathbf{x}_0$  ensures that the model output matches the clean image when the noise level is zero. Together, the differential form in Eq. (9) and the boundary condition define the *differential consistency condition* in Eq. (10), or **consistency condition** in short.

**Finite Difference Approximation.** To learn the consistency condition, we discretize the differential form  $\frac{df}{dt} = 0$  using a finite-difference approximation:

$$0 = \frac{df}{dt} \approx \frac{f_\theta(\mathbf{x}_t) - f_\theta(\mathbf{x}_r)}{t - r} \quad (11)$$

where  $dt \approx \Delta t = t - r$ ,  $t > r > 0$ , and  $f_\theta(\mathbf{x}_t)$  denotes  $f_\theta(\mathbf{x}_t, t)$ . For a given clean image  $\mathbf{x}_0$ , we produce two perturbed images  $\mathbf{x}_t$  and  $\mathbf{x}_r$  using the same perturbation direction  $\epsilon \sim p(\epsilon)$  at two noise levels  $t$  and  $r$ . Specifically, we compute  $t$  and  $r$  according to the forward process of CMs i.e.,  $\mathbf{x}_t = \mathbf{x}_0 + t \cdot \epsilon$  and  $\mathbf{x}_r = \mathbf{x}_0 + r \cdot \epsilon$ .

To satisfy the consistency condition, we minimize the distance between  $f_\theta(\mathbf{x}_t)$  and  $f_\theta(\mathbf{x}_r)$ . For the boundary condition, we optimize  $f_\theta(\mathbf{x}_t)$  to align with the clean image  $\mathbf{x}_0$ . For noise levels  $t > r > 0$ , we freeze  $f_{\text{sg}(\theta)}(\mathbf{x}_r)$  using the stop-gradient operator  $\text{sg}$  and optimize  $f_\theta(\mathbf{x}_t)$  on higher variance inputs to align with self teacher’s prediction  $f_{\text{sg}(\theta)}(\mathbf{x}_r)$  on lower variance inputs (Chen and He, 2021).

**Loss Function.** Given the discretization, the training objective for CMs can be formulated as:

$$\arg \min_{\theta} \mathbb{E}_{\mathbf{x}_0, \epsilon, t} [w(t, r) \mathbf{d}(f_\theta(\mathbf{x}_t), f_{\text{sg}(\theta)}(\mathbf{x}_r))], \quad (12)$$

where we can extract a weighting function  $w(t, r) = \frac{1}{t-r}$ ,  $\mathbf{x}_t = \mathbf{x}_0 + t \cdot \epsilon$ ,  $\mathbf{x}_r = \mathbf{x}_0 + r \cdot \epsilon$  using a *shared noise direction*  $\epsilon \sim p(\epsilon)$ , and  $\mathbf{d}(\cdot, \cdot)$  is a metric function. This formulation generalizes Song et al. (2023)’s discrete training schedule to continuous time. To regularize the model, dropout masks should also be consistent across  $f_\theta(\mathbf{x}_t)$  and  $f_\theta(\mathbf{x}_r)$  by setting a shared random seed, ensuring that the noise levels  $t$  and  $r$  are the only varying factors.

### 3.2 THE "CURSE OF CONSISTENCY" AND ITS IMPLICATIONS

The objective in Eq. (12) can be challenging to optimize when  $\Delta t \rightarrow 0$ . This is because the prediction errors from each discretization interval accumulate, leading to slow training convergence or, in the worst case, divergence. To further elaborate, consider a large noise level  $T$ . We first follow the notation of CT (Song et al., 2023) and split the noise horizon  $[0, T]$  into  $N$  smaller consecutive subintervals. We can error bound the error of 1-step prediction as

$$\|f_\theta(\mathbf{x}_T) - \mathbf{x}_0\| \leq \sum_i^N \|f_\theta(\mathbf{x}_{t_i}) - f_\theta(\mathbf{x}_{r_i})\| \leq N e_{\max}, \quad (13)$$

where  $r_1 = 0 < t_1 = r_2 < \dots < t_{N-2} = r_N < t_N = T$ , and  $e_{\max} = \max_i \|f_\theta(\mathbf{x}_{t_i}) - f_\theta(\mathbf{x}_{r_i})\|$ , for  $i = 1, \dots, N$ . Ideally, we want both  $N$  and  $e_{\max}$  to be small so that this upper bound is small. But in practice, there is a trade-off between these two terms. As  $\Delta t_i = (t_i - r_i) \rightarrow 0$ ,  $e_{\max}$  decreases because  $\mathbf{x}_{t_i}$  and  $\mathbf{x}_{r_i}$  will be close, and it is easier to predict both  $f_\theta(\mathbf{x}_{r_i})$  and  $f_\theta(\mathbf{x}_{t_i})$ . However,  $N$  will increase as  $\Delta t_i \rightarrow 0$ . In contrast, for a large  $\Delta t_i$ , vice-versa holds true. It is difficult to theoretically estimate the rate at which  $e_{\max}$  decreases when  $\Delta t_i = t_i - r_i \rightarrow 0$ , as it depends on the optimization process—specifically, how effectively we train the model to minimize the consistency error in each interval. If  $e_{\max}$  decreases more slowly than  $N$ , the product of the two can increase instead, resulting in a worse prediction error  $\|f_\theta(\mathbf{x}_T) - \mathbf{x}_0\|$ .

The insight from the above observation is that when training from scratch by strictly following the differential form  $\mathrm{d}f/\mathrm{d}t = 0$  with a tiny  $\Delta t_i \approx 0$ , the resulting model might converge slowly due to accumulated consistency errors from each interval  $\Delta t_i$ . To investigate this hypothesis, we conducted experiments training a series of CMs using different fixed numbers of intervals  $N$ , and corresponding  $\Delta t$  values for the consistency condition, as illustrated in Fig. 1. Our observations align with Song and Dhariwal (2023), with the key distinction that we use a fixed  $N$  for this analysis, as this approach provides better insight on how much the precise approximation of the differential consistency condition matters and isolates the effect of discretization errors.

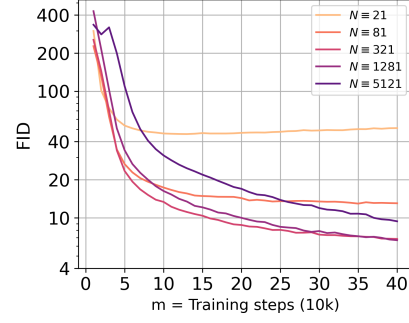


Figure 1: The "Curse of Consistency": The consistency condition holds at  $\Delta t = \mathrm{d}t$ . However, the training dynamics converges more slowly and is less stable as  $\Delta t \rightarrow \mathrm{d}t$  (*i.e.*,  $N \rightarrow \infty$ ).

### 3.3 EASY CONSISTENCY TUNING (ECT)

The discussion in Sec. 3.2 highlighted the training instability issue that can arise when we naively train CMs from scratch and directly optimize for the differential consistency condition with the loss objective in Eq. (12) while directly following  $\Delta t \approx 0$ . In this section, we propose several strategies that largely alleviate the aforementioned training issues and improve the efficiency of CMs. We term this approach Easy Consistency Tuning (ECT), as it effectively balances training stability and model performance while simplifying the CM training process. ECT follows a two-stage approach: diffusion pretraining, followed by consistency tuning, which we will detail in the following subsections.

**Diffusion Pretraining + Consistency Tuning.** Drawing inspiration from iCT’s adaptive discrete-time schedule (Song and Dhariwal, 2023), we start ECT with a large  $\Delta t$ , and gradually shrink  $\Delta t \rightarrow 0$ . In our problem setup, Since  $t > r \geq 0$ , we have the largest possible  $\Delta t = t$  with  $r = 0$ , which yields

$$\arg \min_{\theta} \|f_\theta(\mathbf{x}_t) - f_{\text{sg}(\theta)}(\mathbf{x}_r)\| = \|f_\theta(\mathbf{x}_t) - f_{\text{sg}(\theta)}(\mathbf{x}_0)\| = \|f_\theta(\mathbf{x}_t) - \mathbf{x}_0\|. \quad (14)$$

Training a model with this loss is *identical* to diffusion model/Score SDE (Ho et al., 2020; Song et al., 2021b). This observation suggests a learning scheme that smoothly interpolates from DMs  $\Delta t = t$  to CMs  $\Delta t = \mathrm{d}t$  by gradually shrinking  $\Delta t \rightarrow \mathrm{d}t$  during training by gradually tightening the consistency condition. With this reasoning, diffusion pretraining can be considered as a special case of consistency training with a loose discretization of the consistency condition. Therefore, in practice, we start ECT with a pretrained diffusion model, resulting in a training scheme of pretraining+tuning. Another benefit of this initialization is that during training, especially in the initial stages, it ensures good targets  $f_{\text{sg}(\theta)}(\mathbf{x}_r)$  in the loss objective, avoiding trivial solutions.

We highlight two advantages of this learning scheme: 1. The pretraining+tuning scheme of ECT outperforms iCT’s training-from-scratch approach with lower overall computational cost (see Sec. 4.1). 2. Tuning serves as an efficient proxy for exploring the CM design space. Given a pretrained diffusion model, insights gained during tuning can be applied to improve the pretraining stage, resulting in a more refined overall CM training pipeline. Please refer to Appendix B for more details.

**Continuous-time Training Schedule.** We investigate the design principles of a continuous-time schedule whose "boundary" condition yields standard diffusion pretraining, *i.e.*, constructing training

**Algorithm 1** Easy Consistency Tuning (ECT)

---

**Input:** Dataset  $\mathcal{D}$ , a pretrained diffusion model  $\phi$ , mapping function  $p(r \mid t, \text{Iters})$ , weighting function  $w(t)$ .  
**Init:**  $\theta \leftarrow \theta_\phi$ ,  $\text{Iters} = 0$ .  
**repeat**  
    Sample  $\mathbf{x}_0 \sim \mathcal{D}$ ,  $\epsilon \sim p(\epsilon)$ ,  $t \sim p(t)$ ,  $r \sim p(r \mid t, \text{Iters})$   
    Compute  $\mathbf{x}_t = \mathbf{x}_0 + t \cdot \epsilon$ ,  $\mathbf{x}_r = \mathbf{x}_0 + r \cdot \epsilon$ ,  $\Delta t = t - r$   
     $L(\theta) = w(t) \cdot \mathbf{d}(f_\theta(\mathbf{x}_t), f_{\text{sg}(\theta)}(\mathbf{x}_r))$   $\triangleright$  sg is stop-gradient operator  
     $\theta \leftarrow \theta - \eta \nabla_\theta L(\theta)$   
     $\text{Iters} = \text{Iters} + 1$   
**until**  $\Delta t \rightarrow dt$  **return**  $\theta$   $\triangleright$  ECM

---

pairs of  $r = 0$  for all  $t$  at the beginning. Note that this is unlike the discrete-time schedule used in iCT (See Sec. 2 and Appendix A). We consider overlapped intervals for consistency models, which allows for factoring  $p(t, r) = p(t) p(r|t)$  and continuous sampling of infinite  $t$  from noise distribution  $p(t)$ , for instance,  $\text{LogNormal}(P_{\text{mean}}, P_{\text{std}})$ , and  $r \sim p(r|t)$ .

We refer to  $p(r|t)$  as the mapping function. Since we need to shrink  $\Delta t \rightarrow dt$  as the training progresses, we augment the mapping function to depend on training iterations,  $p(r|t, \text{iters})$ , to control  $\Delta t = (t - r) \rightarrow dt$ . We parametrize the mapping function  $p(r|t, \text{iters})$  as

$$\frac{r}{t} = 1 - \frac{1}{q^a} n(t) = 1 - \frac{1}{q^{\lfloor \text{iters}/d \rfloor}} n(t), \quad (15)$$

where we take  $n(t) = 1 + k \sigma(-bt) = 1 + \frac{k}{1+e^{bt}}$  with  $\sigma(\cdot)$  as the sigmoid function,  $\text{iters}$  refers to training iterations. In general, we set  $q > 1$ ,  $k = 8$  and  $b = 1$ . Since  $r \geq 0$ , we also clamp  $r$  to satisfy this constraint. At the beginning of training, this mapping function produces  $r/t = 0$ , which recovers the diffusion pretraining. We discuss design choices of this function in Appendix A.

**Choice of metric.** iCT uses the Pseudo-Huber metric (Charbonnier et al., 1997) to mitigate the perceptual bias caused by the LPIPS metric (Zhang et al., 2018). When taking a careful look at this metric, we reveal that this metric offers adaptive per-sample scaling of the gradients, which reduces the variance of gradients during training. Specifically, the differential of the Pseudo-Huber loss can be decomposed into two terms: an adaptive scaling factor  $w(\Delta)$  and the differential of the squared  $L_2$  loss. We discuss this in more detail in Appendix A. Thus, we disentangle the weighting function from the loss metric as it provides greater flexibility. In our experiments, we retain the squared  $L_2$  metric used in DMs and explore alternate choices of adaptive weighting terms that reduce the variance of gradients during training. Please refer to Appendix B for further discussions.

**Weighting function.** Weighting functions usually lead to a substantial difference in performance in DMs, and the same holds true for CMs. Substituting the mapping function  $p(r|t)$  in Eq. (15) into the weighting function in Eq. (12), we get  $w(t, r) = 1/(t-r) = q^a \cdot 1/t n(t)$ , where  $q^a$  is the scaling factor to maintain the loss scales when  $\Delta t \rightarrow 0$ , and  $1/t n(t)$  is the weighting akin to DMs. This couples the weighting function with the mapping function  $p(r|t)$ . Instead, we consider decoupled weighting functions without relying on  $p(r|t)$ . Motivated by the adaptive scaling factor that appears in Pseudo-Huber loss (See Appendix A for more details), we rewrite the weighting function as

$$w(t) = \bar{w}(t) \cdot w(\Delta) = \bar{w}(t) \cdot \frac{1}{(\|\Delta\|_2^2 + c^2)^{1/2}}, \quad (16)$$

where  $\Delta = f(\mathbf{x}_t) - f(\mathbf{x}_r)$ . We define  $\bar{w}(t)$  as timestep weighting, while  $w(\Delta)$  as adaptive weighting. The adaptive weighting improves training efficiency with the  $L_2$  metric because, as  $\Delta \rightarrow 0$  (usually happens when  $t \rightarrow 0$ ), this weighting  $w(\Delta)$  upscales gradients to avoid vanishing gradient during learning of fine-grained features, while  $c$  mitigates potential numerical issues when  $\Delta \approx 0$ . We direct the reader to Tab. 2 in Appendix B for a detailed overview of various choices of  $\bar{w}(t)$  and  $w(\Delta)$  considered in this work. In general, we notice that CMs’ generative capability greatly benefits from weighting functions that control the variance of the gradients across different noise levels. We provide a brief summary of the core steps of ECT in Alg. 1.

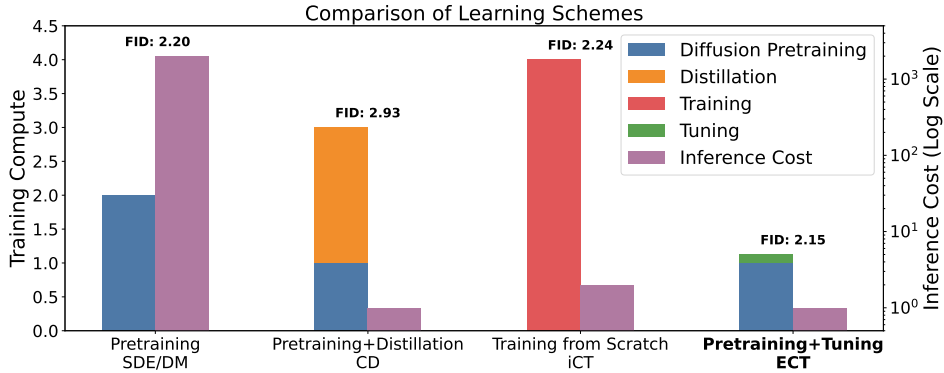


Figure 2: Comparison of training schemes for the diffusion-consistency family on CIFAR-10. Without relying on distillation from frozen diffusion teachers or extra adversarial supervision, ECT surpasses Consistency Distillation (CD) (Song et al., 2023) and Consistency Models trained from scratch (iCT) (Song and Dhariwal, 2023) using  $1/4$  of the total training cost. ECT also significantly reduces the inference cost to  $1/1000$  compared to Diffusion Pretraining (Score SDE/DMs) while maintaining comparable sample quality.



Figure 3: Scaling up training compute and model sizes results in improved sample quality on ImageNet  $64 \times 64$ . Each triplet (left-to-right) has 2-step samples from ECM-S trained with 12.8M images, ECM-S trained with 102.4M images, and ECM-XL trained with 102.4M images.

## 4 EXPERIMENTS

This section compares different learning schemes and investigates scaling laws of ECT, while more experiments on design choices and scaling are shown in Appendix B. We evaluate the efficiency and scalability of ECT on two datasets: CIFAR-10 (Krizhevsky, 2009) and ImageNet  $64 \times 64$  (Deng et al., 2009). We measure the sample quality using Fréchet Inception Distance (FID) (Heusel et al., 2017) and Fréchet Distance under the DINOv2 model (Oquab et al., 2023) ( $FD_{DINOv2}$ ) (Stein et al., 2024) and sampling efficiency using the number of function evaluations (NFEs). We also indicate the relative training costs of each of these methods. Implementation details can be found in Appendix D.

### 4.1 COMPARISON OF TRAINING SCHEMES

We compare CMs trained with ECT (denoted as ECM) against state-of-the-art diffusion models, advanced samplers for diffusion models, distillation methods such as consistency distillation (CD) (Song et al., 2023), and improved Consistency Training (iCT) (Song and Dhariwal, 2023). The key results are summarized in Fig. 2. We show the training FLOPs, inference cost, and generative performance of the four training schemes.

**Score SDE/Diffusion Models.** We compare ECMs against Score SDE (Song et al., 2021b), EDM (Karras et al., 2022), and EDM with DPM-Solver-v3 (Zheng et al., 2024). 2-step ECM, which has

Table 1: Generative performance on unconditional CIFAR-10 and class-conditional ImageNet  $64 \times 64$ . We use a budget of 12.8M training images (batch size 128 and 100k iterations) for ECMs. \* stands for a budget of 102.4M training images (batch size 1024 and 100k iterations) on ImageNet  $64 \times 64$ .

CIFAR-10			ImageNet $64 \times 64$		
Method	FID↓	NFE↓	Method	FID↓	NFE↓
Diffusion Models			Diffusion Models		
Score SDE (Song et al., 2020)	2.38	2000	ADM (Karras et al., 2022)	2.07	250
Score SDE-deep (Song et al., 2020)	2.20	2000	EDM (Karras et al., 2022)	2.22	79
EDM (Karras et al., 2022)	2.01	35	EDM2-XL (Karras et al., 2023)	1.33	63
EDM (DPM-Solver-v3) (Zheng et al., 2024)	2.51	10	Diffusion Distillation		
Diffusion Distillation			BOOT (Gu et al., 2023)	16.3	1
PD (Salimans and Ho, 2022)	8.34	1	DFNO (LPIPS) (Zheng et al., 2023)	7.83	1
GET (Geng et al., 2024)	5.49	1	Diff-Instruct (Luo et al., 2024)	5.57	1
Diff-Instruct (Luo et al., 2024)	4.53	1	TRACT (Berthelot et al., 2023)	4.97	2
TRACT (Berthelot et al., 2023)	3.32	2	PD (LPIPS) (Salimans and Ho, 2022)	5.74	2
CD (LPIPS) (Song et al., 2023)	3.55	1	CD (LPIPS) (Song et al., 2023)	4.70	2
CD (LPIPS) (Song et al., 2023)	2.93	2	Consistency Models		
Consistency Models			iCT (Song and Dhariwal, 2023)	3.20	2
iCT (Song and Dhariwal, 2023)	2.83	1	iCT-deep (Song and Dhariwal, 2023)	2.77	2
	2.46	2	ECT		
iCT-deep (Song and Dhariwal, 2023)	2.51	1	ECM-S (100k iters)	3.18	2
	2.24	2	ECM-M (100k iters)	2.35	2
ECT			ECM-L (100k iters)	2.14	2
ECM (100k iters)	4.54	1	ECM-XL (100k iters)	1.96	2
ECM (200k iters)	3.86	1	ECM-S*	4.05	1
ECM (400k iters)	3.60	1	ECM-S*	2.79	2
ECM (100k iters)	2.20	2	ECM-XL*	2.49	1
ECM (200k iters)	2.15	2	ECM-XL*	1.67	2
ECM (400k iters)	2.11	2			

been fine-tuned for only 100k iterations, matches Score SDE-deep, with  $2 \times$  model depth and 2000 NFEs, in terms of FID. As noted in Fig. 2, ECM only requires  $1/1000$  of its inference cost and latency to achieve the same sample quality. 2-step ECM fine-tuned for 100k iterations outperforms EDM with advanced DPM-Solver-v3 (NFE=10).

**Diffusion Distillation.** We compare ECT against Consistency Distillation (CD) (Song et al., 2023), a SoTA approach that distills a pretrained DM into a CM. As shown in Tab. 1, ECM significantly outperforms CD on both CIFAR-10 and ImageNet  $64 \times 64$ . We note that ECT is free from the errors of teacher DM and does not incur any additional cost of running teacher DM. 2-step ECM outperforms 2-step CD (with LPIPS (Zhang et al., 2018)) in terms of FID (2.20 vs 2.93) on CIFAR-10 while using around  $1/3$  of training compute of CD.

**Consistency training from scratch.** Improved Consistency Training (iCT) (Song and Dhariwal, 2023) is the SoTA recipe for training a consistency model from scratch without inferring the diffusion teacher. Compared to training from scratch, ECT rivals iCT-deep using  $1/4$  of the overall training compute ( $1/8$  in the tuning stage) and  $1/2$  of the model size as shown in Fig. 2 and Tab. 1.

## 4.2 SCALING LAWS OF ECT

We leverage efficiency of ECT to examine the scaling behavior of CMs, including training compute, model size, and model FLOPs. We find that when computational resources are not a bottleneck, ECT scales well and follows the classic power law.

**Training Compute.** Initializing from the weights of EDM (Karras et al., 2022), we fine-tune ECMs across six compute scales on CIFAR-10 (Krizhevsky, 2009) and plot the trend of  $FD_{DINOv2}$  against training compute in Fig. 4 (Left). The largest compute reaches  $2 \times$  the diffusion pretraining budget. As we scale up the training budget, we observe a classic power-law decay in  $FD_{DINOv2}$ , indicating that increased computational investment in ECT leads to substantial improvements in generative performance. Intriguingly, the gap between 1-step and 2-step generation becomes *narrower* when

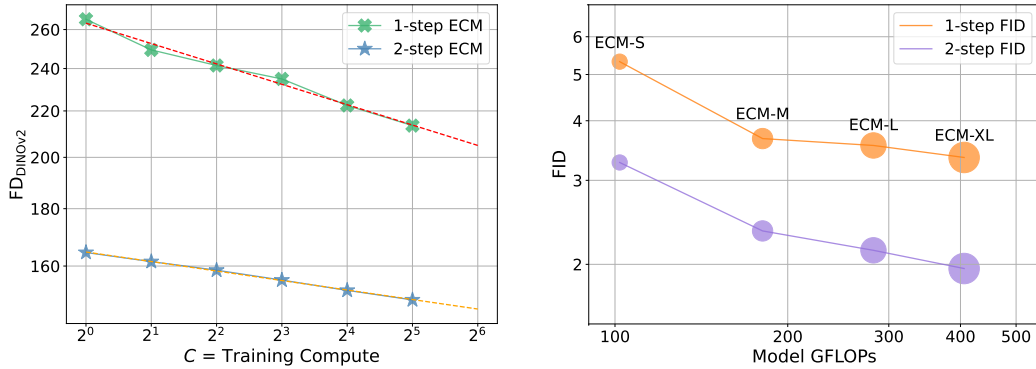


Figure 4: (Left): Scaling up training compute yields the classic power-law between  $FD_{DINOv2} \downarrow$  and training compute, with  $K = 263$ ,  $\alpha = -0.060$  for 1-step inference, and  $K = 164$ ,  $\alpha = -0.028$  for 2-step inference, (Right): Given the same batch size and iterations, scaling up model sizes and model FLOPs strongly correlates with FID  $\downarrow$  improvements on ImageNet  $64 \times 64$ . The diameter is proportional to the model size.

scaling up training compute, even while using the same  $\Delta t \rightarrow dt$  schedule. We further fit the power-law  $FD_{DINOv2} = K \cdot C^\alpha$ , where  $C$  is the normalized training FLOPs. The Pearson correlation coefficient between  $\log(\text{Training Compute})$  and  $\log(FD_{DINOv2})$  for 1-step and 2-step generation is  $-0.9940$  and  $-0.9996$ , respectively, both with statistical significance ( $p$ -values  $< 10^{-4}$ ).

**Model Size & FLOPs.** Initialized from EDM2 (Karras et al., 2024) pretraining, we train ECM-S/M/L/XL models with parameters from 280M to 1.1B and model FLOPs from 102G to 406G. As demonstrated in Fig. 4, both 1-step and 2-step generation capabilities exhibit log-linear scaling for model FLOPs and parameters. This scaling behavior confirms that ECT effectively leverages increased model sizes and computational power to improve 1-step and 2-step generative capabilities.

Notably, ECT achieves *better* 2-step generation performance than state-of-the-art CMs, while utilizing only **33%** of the overall computational budget compared to iCT (Song and Dhariwal, 2023) (batch size  $4096 \times 800k$ ). This significant efficiency is achieved through a two-stage process: pre-training and tuning. While the pretraining stage utilizes the EDM2 pipeline, the tuning stage of ECT requires a remarkably modest budget of 12.8M training images (batch size  $128 \times 100k$ ), ranging from **0.60%** to **1.91%** of the pretraining budget, depending on the model sizes.

**Inference.** Our scaling study also indicates a sweet spot for the inference of CMs. On both CIFAR-10 and ImageNet  $64 \times 64$ , there are 2-step inferences of smaller models surpassing 1-step inferences of larger models, *e.g.*, 498M ECM-M against 1.1B ECM-XL. This calls for further studies of inference-optimal scaling and test-time compute scaling for visual generation.

## 5 RELATED WORK

**Consistency Models.** Consistency models (Song et al., 2023; Song and Dhariwal, 2023) are a new family of generative models designed for efficient generation with few model steps without the need for adversarial training. CMs do not rely on a pretrained diffusion model (DM) to generate training targets but instead leverage an unbiased score estimator. Training CMs have been extended to multi-step sampling (Kim et al., 2024; Wang et al., 2024b; Heek et al., 2024), latent space models (Luo et al., 2023), ControlNet (Xiao et al., 2023), video (Wang et al., 2024c), and combined with an additional adversarial loss (Kim et al., 2024; Kong et al., 2023). Despite their sampling efficiency, CMs are typically more challenging to train and require significantly more compute resources than their diffusion counterparts. Our work substantially improves the training efficiency of CMs, reducing the cost of future research and deployment on CMs. Parallel to our work, Wang et al. (2024b); Heek et al. (2024) relax the single-step constraint of CMs and generalize them to multi-step variants, drawing inspiration from TRACT (Berthelot et al., 2023). Under the piecewise linear design, increasing the number of segments will also lead to diffusion pretraining, showing a different approach to connect CMs to the standard diffusion models.

**Diffusion Distillation.** Drawing inspiration from knowledge distillation (Hinton et al., 2015), distillation is the most widespread training-based approach to accelerate the diffusion sampling procedure. In diffusion distillation, a pretrained diffusion model (DM), which requires hundreds to thousands of model evaluations to generate samples, acts as a teacher. A student model is trained to match the teacher model’s sample quality, enabling it to generate high-quality samples in a few steps.

There are two main lines of work in this area. The first category involves trajectory matching, where the student learns to match points on the teacher’s sampling trajectory. Methods in this category include offline distillation (Luhman and Luhman, 2021; Geng et al., 2024; Zheng et al., 2023), which require an offline synthetic dataset generated by sampling from a pretrained DM to distill a teacher model into a few-step student model; progressive distillation (Salimans and Ho, 2022; Meng et al., 2023), and TRACT (Berthelot et al., 2023), which require multiple training passes or offline datasets to achieve the same goal; and BOOT (Gu et al., 2023), Consistency Distillation (CD) (Song et al., 2023), and Imagine-Flash (Kohler et al., 2024), which minimize the difference between the student predictions at carefully selected points on the sampling trajectory.

CD is closely related to our method, as it leverages a teacher model to generate pairs of adjacent points and enforces the student predictions at these points to map to the initial data point. However, it employs a fixed schedule derived from a specific sampler, which may introduce non-negligible discretization errors in approximating the consistency condition. It also limits the quality of consistency models to that of the pretrained diffusion model.

The second category minimizes the probabilistic divergence between data and model distributions, *i.e.*, distribution matching (Poole et al., 2022; Wang et al., 2024a; Luo et al., 2024; Yin et al., 2023; Zhou et al., 2024a). These methods (Luo et al., 2024; Sauer et al., 2023; Yin et al., 2023; Nguyen and Tran, 2023; Kohler et al., 2024; Xu et al., 2023a; Lin et al., 2024; Zhou et al., 2024b) use score distillation or adversarial loss, to distill an expensive teacher model into an efficient student model. However, they can be challenging to train in a stable manner due to the alternating updating schemes from either adversarial or score distillation. Some of these methods such as DreamFusion (Poole et al., 2022) and ProlificDreamer (Wang et al., 2024a) are used for 3D object generation.

A drawback of training-based approaches is that they need additional training procedures after pretraining to distill an efficient student, which can be computationally intensive. For a detailed discussion on the recent progress of diffusion distillation, we direct the readers to Dieleman (2024).

**Fast Samplers for Diffusion Models.** Fast samplers are usually training-free and use advanced solvers to simulate the diffusion stochastic differential equation (SDE) or ordinary differential equation (ODE) to reduce the number of sampling steps. These methods reduce the discretization error during sampling by analytically solving a part of SDE or ODE (Lu et al., 2022a; Xue et al., 2024; Lu et al., 2022b), by using exponential integrators and higher order polynomials for better approximation of the solution (Zhang and Chen, 2022), using higher order numerical methods (Karras et al., 2022), using better approximation of noise levels during sampling (Kong and Ping, 2021), correcting predictions at each step of sampling (Zhao et al., 2024) and ensuring that the solution of the ODE lies on a desired manifold (Liu et al., 2022a). Another orthogonal strategy is the parallel sampling process (Pokle et al., 2022; Shih et al., 2024), solving fixed points of the entire ODE/SDE trajectories. A drawback of these fast samplers is that the quality of samples drastically reduces as the number of sampling steps falls below a threshold such as 10 steps.

## 6 CONCLUSION

We propose Easy Consistency Tuning (ECT), a simple yet efficient scheme for training consistency models. The resulting models, ECMs, unlock state-of-the-art few-step generative capabilities at a minimal tuning cost and are able to benefit from scaling. We have made our `code` available to ease future prototyping, studying, and deploying consistency models within the community.

## 7 LIMITATIONS

One of the major limitations of ECT is that it requires a dataset to tune DMs to CMs. Recent works developed data-free approaches (Luo et al., 2024; Gu et al., 2023; Yin et al., 2023; Zhou et al., 2024a) for diffusion distillation. The distinction between ECT and data-free methods is that ECT learns the

*consistency condition* on a given dataset through the self teacher, while data-free methods transfer knowledge from a frozen diffusion teacher. This feature of ECT can be a potential limitation since the training data of bespoke models are unavailable to the public. However, we hold an optimistic view on tuning CMs using datasets different from pretraining.

In Appendix C, we discuss a data-free variant of Easy Consistency Distillation (ECD), in which we extend the continuous time formulation to Consistency Distillation, by generating self-synthetic data from CM on-the-fly. However, it only applies to the distillation settings. Further data-centric research is needed regarding synthetic data, data composition, and data scaling for consistency models.

## BROADER IMPACTS AND ETHICS STATEMENT

We propose Easy Consistency Tuning (ECT) that can efficiently train consistency models as state-of-the-art few-step generators, using only a small fraction of the computational requirements compared to current CMs training and diffusion distillation methods. We hope that ECT will democratize the creation of high-quality generative models, enabling artists and creators to produce content more efficiently. While this advancement can aid creative industries by reducing computational costs and speeding up workflows, it also raises concerns about the potential misuse of generative models to produce misleading, fake, or biased content. We conduct experiments on academic benchmarks, whose resulting models are less likely to be misused. Further experiments are needed to better understand these consistency model limitations and propose solutions to address them.

## REPRODUCIBILITY STATEMENT

We provide extensive details of experimental settings and hyperparameters to reproduce our experimental results in Appendix D. We have provided a zip file of our source code in this submission. We plan to release our code to ensure transparency and reproducibility of the results.

## ACKNOWLEDGMENTS

Zhengyang Geng and Ashwini Pople are supported by funding from the Bosch Center for AI. Zico Kolter gratefully acknowledges Bosch’s funding for the lab. The FLAME Center at CMU generously supports this research.

We appreciate Yang Song for discussions and feedback. We acknowledge the discussions and comments provided by Tianle Cai, Antony Jia, Diyang Xue, Runtian Zhai, and Yonghao Zhuang during the preparation of the [blog post](#).

## REFERENCES

- Jonathan Ho, Ajay Jain, and Pieter Abbeel. Denoising diffusion probabilistic models. *Neural Information Processing Systems (NeurIPS)*, 33, 2020. [1](#), [5](#)
- Jiaming Song, Chenlin Meng, and Stefano Ermon. Denoising diffusion implicit models. In *International Conference on Learning Representations (ICLR)*, 2021a. [1](#)
- Yang Song, Jascha Sohl-Dickstein, Diederik P Kingma, Abhishek Kumar, Stefano Ermon, and Ben Poole. Score-based generative modeling through stochastic differential equations. *arXiv preprint arXiv:2011.13456*, 2020. [1](#), [8](#)
- Yang Song, Jascha Sohl-Dickstein, Diederik P Kingma, Abhishek Kumar, Stefano Ermon, and Ben Poole. Score-based generative modeling through stochastic differential equations. In *International Conference on Learning Representations (ICLR)*, 2021b. [1](#), [2](#), [5](#), [7](#), [24](#)
- Robin Rombach, Andreas Blattmann, Dominik Lorenz, Patrick Esser, and Björn Ommer. High-resolution image synthesis with latent diffusion models. 2022 ieee. In *CVF Conference on Computer Vision and Pattern Recognition (CVPR)*, pages 10674–10685, 2021. [1](#)

- Chitwan Saharia, Jonathan Ho, William Chan, Tim Salimans, David J Fleet, and Mohammad Norouzi. Image super-resolution via iterative refinement. *IEEE transactions on pattern analysis and machine intelligence*, 45(4):4713–4726, 2022. [1](#)
- Jonathan Ho, Chitwan Saharia, William Chan, David J Fleet, Mohammad Norouzi, and Tim Salimans. Cascaded diffusion models for high fidelity image generation. *Journal of Machine Learning Research*, 2022a. [1](#)
- Prafulla Dhariwal and Alexander Nichol. Diffusion models beat gans on image synthesis. *Neural Information Processing Systems (NeurIPS)*, 34, 2021. [1](#)
- Ali Hatamizadeh, Jiaming Song, Guilin Liu, Jan Kautz, and Arash Vahdat. Diffit: Diffusion vision transformers for image generation. *arXiv preprint arXiv:2312.02139*, 2023. [1](#)
- Aditya Ramesh, Mikhail Pavlov, Gabriel Goh, Scott Gray, Chelsea Voss, Alec Radford, Mark Chen, and Ilya Sutskever. Zero-shot text-to-image generation. In *International Conference on Machine Learning (ICML)*, 2021. [1](#)
- Tim Brooks, Bill Peebles, Connor Homes, Will DePue, Yufei Guo, Li Jing, David Schnurr, Joe Taylor, Troy Luhman, Eric Luhman, Clarence Wing Yin Ng, Ricky Wang, and Aditya Ramesh. Video generation models as world simulators. 2024. [1](#)
- Andreas Blattmann, Tim Dockhorn, Sumith Kulal, Daniel Mendelevitch, Maciej Kilian, Dominik Lorenz, Yam Levi, Zion English, Vikram Voleti, Adam Letts, et al. Stable video diffusion: Scaling latent video diffusion models to large datasets. *arXiv preprint arXiv:2311.15127*, 2023. [1](#)
- Omer Bar-Tal, Hila Chefer, Omer Tov, Charles Herrmann, Roni Paiss, Shiran Zada, Ariel Ephrat, Junhwa Hur, Yuanzhen Li, Tomer Michaeli, et al. Lumiere: A space-time diffusion model for video generation. *arXiv preprint arXiv:2401.12945*, 2024. [1](#)
- Jonathan Ho, William Chan, Chitwan Saharia, Jay Whang, Ruiqi Gao, Alexey Gritsenko, Diederik P Kingma, Ben Poole, Mohammad Norouzi, David J Fleet, et al. Imagen video: High definition video generation with diffusion models. *arXiv preprint arXiv:2210.02303*, 2022b. [1](#)
- Agrim Gupta, Lijun Yu, Kihyuk Sohn, Xiuye Gu, Meera Hahn, Li Fei-Fei, Irfan Essa, Lu Jiang, and José Lezama. Photorealistic video generation with diffusion models. *arXiv preprint arXiv:2312.06662*, 2023. [1](#)
- Ben Poole, Ajay Jain, Jonathan T Barron, and Ben Mildenhall. Dreamfusion: Text-to-3d using 2d diffusion. *arXiv preprint arXiv:2209.14988*, 2022. [1](#), [10](#)
- Zhengyi Wang, Cheng Lu, Yikai Wang, Fan Bao, Chongxuan Li, Hang Su, and Jun Zhu. Pro-lificdreamer: High-fidelity and diverse text-to-3d generation with variational score distillation. *Advances in Neural Information Processing Systems*, 36, 2024a. [1](#), [10](#)
- Kyungmin Lee, Kihyuk Sohn, and Jinwoo Shin. Dreamflow: High-quality text-to-3d generation by approximating probability flow. *arXiv preprint arXiv:2403.14966*, 2024. [1](#)
- Yang Chen, Yingwei Pan, Haibo Yang, Ting Yao, and Tao Mei. Vp3d: Unleashing 2d visual prompt for text-to-3d generation. *arXiv preprint arXiv:2403.17001*, 2024. [1](#)
- Sudarshan Babu, Richard Liu, Avery Zhou, Michael Maire, Greg Shakhnarovich, and Rana Hanocka. Hyperfields: Towards zero-shot generation of nerfs from text. *arXiv preprint arXiv:2310.17075*, 2023. [1](#)
- Tero Karras, Miika Aittala, Timo Aila, and Samuli Laine. Elucidating the design space of diffusion-based generative models. In *Proc. NeurIPS*, 2022. [1](#), [2](#), [3](#), [7](#), [8](#), [10](#), [18](#), [20](#), [22](#), [24](#)
- Eric Luhman and Troy Luhman. Knowledge distillation in iterative generative models for improved sampling speed. *ArXiv*, abs/2101.02388, 2021. [1](#), [10](#), [24](#)
- Tim Salimans and Jonathan Ho. Progressive distillation for fast sampling of diffusion models. *arXiv preprint arXiv:2202.00512*, 2022. [1](#), [8](#), [10](#), [18](#), [19](#)

- Weijian Luo, Tianyang Hu, Shifeng Zhang, Jiacheng Sun, Zhenguo Li, and Zhihua Zhang. Diff-instruct: A universal approach for transferring knowledge from pre-trained diffusion models. *Neural Information Processing Systems (NeurIPS)*, 2024. 1, 8, 10, 24
- Jiatao Gu, Shuangfei Zhai, Yizhe Zhang, Lingjie Liu, and Joshua M Susskind. Boot: Data-free distillation of denoising diffusion models with bootstrapping. In *ICML 2023 Workshop on Structured Probabilistic Inference & Generative Modeling*, 2023. 1, 8, 10, 24
- Axel Sauer, Dominik Lorenz, Andreas Blattmann, and Robin Rombach. Adversarial diffusion distillation. *arXiv preprint arXiv:2311.17042*, 2023. 1, 10
- Zhengyang Geng, Ashwini Pople, and J Zico Kolter. One-step diffusion distillation via deep equilibrium models. *Neural Information Processing Systems (NeurIPS)*, 36, 2024. 1, 8, 10, 24
- Tianwei Yin, Michaël Gharbi, Richard Zhang, Eli Shechtman, Fredo Durand, William T Freeman, and Taesung Park. One-step diffusion with distribution matching distillation. *arXiv preprint arXiv:2311.18828*, 2023. 1, 10, 24
- Thuan Hoang Nguyen and Anh Tran. Swiftbrush: One-step text-to-image diffusion model with variational score distillation. *arXiv preprint arXiv:2312.05239*, 2023. 1, 10
- Taehong Moon, Moonseok Choi, EungGu Yun, Jongmin Yoon, Gayoung Lee, and Juho Lee. Early exiting for accelerated inference in diffusion models. In *ICML 2023 Workshop on Structured Probabilistic Inference & Generative Modeling*, 2023. 1
- Shengkun Tang, Yaqing Wang, Caiwen Ding, Yi Liang, Yao Li, and Dongkuan Xu. Deediff: Dynamic uncertainty-aware early exiting for accelerating diffusion model generation. *arXiv preprint arXiv:2309.17074*, 2023. 1
- Zhifeng Kong and Wei Ping. On fast sampling of diffusion probabilistic models. *arXiv preprint arXiv:2106.00132*, 2021. 1, 10
- Cheng Lu, Yuhao Zhou, Fan Bao, Jianfei Chen, Chongxuan Li, and Jun Zhu. Dpm-solver: A fast ode solver for diffusion probabilistic model sampling in around 10 steps. *arXiv preprint arXiv:2206.00927*, 2022a. 1, 10
- Qinsheng Zhang and Yongxin Chen. Fast sampling of diffusion models with exponential integrator. *arXiv preprint arXiv:2204.13902*, 2022. 1, 10
- Zhenyu Zhou, Defang Chen, Can Wang, and Chun Chen. Fast ode-based sampling for diffusion models in around 5 steps. *arXiv preprint arXiv:2312.00094*, 2023. 1
- Shuchen Xue, Mingyang Yi, Weijian Luo, Shifeng Zhang, Jiacheng Sun, Zhenguo Li, and Zhi-Ming Ma. Sa-solver: Stochastic adams solver for fast sampling of diffusion models. *Neural Information Processing Systems (NeurIPS)*, 2024. 1, 10
- Zizheng Pan, Bohan Zhuang, De-An Huang, Weili Nie, Zhiding Yu, Chaowei Xiao, Jianfei Cai, and Anima Anandkumar. T-stitch: Accelerating sampling in pre-trained diffusion models with trajectory stitching. *arXiv preprint arXiv:2402.14167*, 2024. 1
- Yang Song, Prafulla Dhariwal, Mark Chen, and Ilya Sutskever. Consistency models. *arXiv preprint arXiv:2303.01469*, 2023. 1, 2, 3, 4, 7, 8, 9, 10, 23, 24
- Yang Song and Prafulla Dhariwal. Improved techniques for training consistency models. *arXiv preprint arXiv:2310.14189*, 2023. 1, 2, 3, 4, 5, 7, 8, 9, 18, 20, 23, 25, 26
- Jia Deng, Wei Dong, Richard Socher, Li-Jia Li, Kai Li, and Li Fei-Fei. Imagenet: A large-scale hierarchical image database. In *2009 IEEE conference on computer vision and pattern recognition*, pages 248–255. Ieee, 2009. 2, 7
- Alex Krizhevsky. Learning multiple layers of features from tiny images. 2009. URL <https://www.cs.toronto.edu/~kriz/cifar.html>. 2, 7, 8

- Richard Zhang, Phillip Isola, Alexei A Efros, Eli Shechtman, and Oliver Wang. The unreasonable effectiveness of deep features as a perceptual metric. In *Proceedings of the IEEE conference on computer vision and pattern recognition*, 2018. 3, 6, 8, 18, 21
- Xinlei Chen and Kaiming He. Exploring simple siamese representation learning. In *Proceedings of the IEEE/CVF conference on computer vision and pattern recognition*, pages 15750–15758, 2021. 4
- Pierre Charbonnier, Laure Blanc-Féraud, Gilles Aubert, and Michel Barlaud. Deterministic edge-preserving regularization in computed imaging. *IEEE Transactions on image processing*, 6(2): 298–311, 1997. 6, 18
- Martin Heusel, Hubert Ramsauer, Thomas Unterthiner, Bernhard Nessler, and Sepp Hochreiter. Gans trained by a two time-scale update rule converge to a local nash equilibrium. *Neural Information Processing Systems (NeurIPS)*, 30, 2017. 7
- Maxime Oquab, Timothée Darcet, Théo Moutakanni, Huy Vo, Marc Szafraniec, Vasil Khalidov, Pierre Fernandez, Daniel Haziza, Francisco Massa, Alaaeldin El-Nouby, et al. Dinov2: Learning robust visual features without supervision. *arXiv preprint arXiv:2304.07193*, 2023. 7, 21
- George Stein, Jesse Cresswell, Rasa Hosseinzadeh, Yi Sui, Brendan Ross, Valentin Vilecroze, Zhaoyan Liu, Anthony L Caterini, Eric Taylor, and Gabriel Loaiza-Ganem. Exposing flaws of generative model evaluation metrics and their unfair treatment of diffusion models. *Advances in Neural Information Processing Systems*, 36, 2024. 7, 21, 25, 26
- Kaiwen Zheng, Cheng Lu, Jianfei Chen, and Jun Zhu. Dpm-solver-v3: Improved diffusion ode solver with empirical model statistics. *Neural Information Processing Systems (NeurIPS)*, 2024. 7, 8
- David Berthelot, Arnaud Autef, Jierui Lin, Dian Ang Yap, Shuangfei Zhai, Siyuan Hu, Daniel Zheng, Walter Talbott, and Eric Gu. Tract: Denoising diffusion models with transitive closure time-distillation. *arXiv preprint arXiv:2303.04248*, 2023. 8, 9, 10
- Tero Karras, Miika Aittala, Jaakko Lehtinen, Janne Hellsten, Timo Aila, and Samuli Laine. Analyzing and improving the training dynamics of diffusion models. *arXiv preprint arXiv:2312.02696*, 2023. 8
- Hongkai Zheng, Weili Nie, Arash Vahdat, Kamyar Azizzadenesheli, and Anima Anandkumar. Fast sampling of diffusion models via operator learning. In *International Conference on Machine Learning (ICML)*. PMLR, 2023. 8, 10, 24
- Tero Karras, Miika Aittala, Jaakko Lehtinen, Janne Hellsten, Timo Aila, and Samuli Laine. Analyzing and improving the training dynamics of diffusion models. In *IEEE Conference on Computer Vision and Pattern Recognition (CVPR)*, 2024. 9, 19, 22, 23, 24, 25, 26
- Dongjun Kim, Chieh-Hsin Lai, Wei-Hsiang Liao, Naoki Murata, Yuhta Takida, Toshimitsu Uesaka, Yutong He, Yuki Mitsufuji, and Stefano Ermon. Consistency trajectory models: Learning probability flow ODE trajectory of diffusion. In *International Conference on Learning Representations (ICLR)*, 2024. 9
- Fu-Yun Wang, Zhaoyang Huang, Alexander William Bergman, Dazhong Shen, Peng Gao, Michael Lingelbach, Keqiang Sun, Weikang Bian, Guanglu Song, Yu Liu, et al. Phased consistency model. *arXiv preprint arXiv:2405.18407*, 2024b. 9
- Jonathan Heek, Emiel Hoogeboom, and Tim Salimans. Multistep consistency models. *arXiv preprint arXiv:2403.06807*, 2024. 9
- Simian Luo, Yiqin Tan, Longbo Huang, Jian Li, and Hang Zhao. Latent consistency models: Synthesizing high-resolution images with few-step inference, 2023. 9
- Jie Xiao, Kai Zhu, Han Zhang, Zhiheng Liu, Yujun Shen, Yu Liu, Xueyang Fu, and Zheng-Jun Zha. Ccm: Adding conditional controls to text-to-image consistency models. *arXiv preprint arXiv:2312.06971*, 2023. 9

- Fu-Yun Wang, Zhaoyang Huang, Xiaoyu Shi, Weikang Bian, Guanglu Song, Yu Liu, and Hongsheng Li. Animate1cm: Accelerating the animation of personalized diffusion models and adapters with decoupled consistency learning. *arXiv preprint arXiv:2402.00769*, 2024c. 9
- Fei Kong, Jinhao Duan, Lichao Sun, Hao Cheng, Renjing Xu, Hengtao Shen, Xiaofeng Zhu, Xiaoshuang Shi, and Kaidi Xu. Act: Adversarial consistency models. *arXiv preprint arXiv:2311.14097*, 2023. 9
- Geoffrey Hinton, Oriol Vinyals, and Jeff Dean. Distilling the knowledge in a neural network. *arXiv preprint arXiv:1503.02531*, 2015. 10
- Chenlin Meng, Robin Rombach, Ruiqi Gao, Diederik Kingma, Stefano Ermon, Jonathan Ho, and Tim Salimans. On distillation of guided diffusion models. In *Proceedings of the IEEE/CVF Conference on Computer Vision and Pattern Recognition*, pages 14297–14306, 2023. 10
- Jonas Kohler, Albert Pumarola, Edgar Schönfeld, Artsiom Sanakoyeu, Roshan Sumbaly, Peter Vajda, and Ali Thabet. Imagine flash: Accelerating emu diffusion models with backward distillation. *arXiv preprint arXiv:2405.05224*, 2024. 10
- Mingyuan Zhou, Huangjie Zheng, Zhendong Wang, Mingzhang Yin, and Hai Huang. Score identity distillation: Exponentially fast distillation of pretrained diffusion models for one-step generation. In *International Conference on Machine Learning*, 2024a. 10, 24
- Yanwu Xu, Yang Zhao, Zhisheng Xiao, and Tingbo Hou. Ufogen: You forward once large scale text-to-image generation via diffusion gans. *arXiv preprint arXiv:2311.09257*, 2023a. 10
- Shanchuan Lin, Anran Wang, and Xiao Yang. Sdxl-lightning: Progressive adversarial diffusion distillation. *arXiv preprint arXiv:2402.13929*, 2024. 10
- Mingyuan Zhou, Zhendong Wang, Huangjie Zheng, and Hai Huang. Long and short guidance in score identity distillation for one-step text-to-image generation. *ArXiv 2406.01561*, 2024b. URL <https://arxiv.org/abs/2406.01561>. 10
- Sander Dieleman. The paradox of diffusion distillation, 2024. URL <https://sander.ai/2024/02/28/paradox.html>. 10
- Cheng Lu, Yuhao Zhou, Fan Bao, Jianfei Chen, Chongxuan Li, and Jun Zhu. Dpm-solver++: Fast solver for guided sampling of diffusion probabilistic models. *arXiv preprint arXiv:2211.01095*, 2022b. 10
- Wenliang Zhao, Lujia Bai, Yongming Rao, Jie Zhou, and Jiwen Lu. Unipc: A unified predictor-corrector framework for fast sampling of diffusion models. *Neural Information Processing Systems (NeurIPS)*, 2024. 10
- Luping Liu, Yi Ren, Zhijie Lin, and Zhou Zhao. Pseudo numerical methods for diffusion models on manifolds. *arXiv preprint arXiv:2202.09778*, 2022a. 10
- Ashwini Pople, Zhengyang Geng, and J Zico Kolter. Deep equilibrium approaches to diffusion models. *Neural Information Processing Systems (NeurIPS)*, 2022. 10
- Andy Shih, Suneel Belkale, Stefano Ermon, Dorsa Sadigh, and Nima Anari. Parallel sampling of diffusion models. *Neural Information Processing Systems (NeurIPS)*, 2024. 10
- Diederik Kingma and Ruiqi Gao. Understanding diffusion objectives as the elbo with simple data augmentation. *Neural Information Processing Systems (NeurIPS)*, 2024. 18
- Tiankai Hang, Shuyang Gu, Chen Li, Jianmin Bao, Dong Chen, Han Hu, Xin Geng, and Baining Guo. Efficient diffusion training via min-snr weighting strategy. In *Proceedings of the IEEE/CVF International Conference on Computer Vision*, pages 7441–7451, 2023. 18
- Katherine Crowson, Stefan Andreas Baumann, Alex Birch, Tanishq Mathew Abraham, Daniel Z Kaplan, and Enrico Shippole. Scalable high-resolution pixel-space image synthesis with hourglass diffusion transformers. *arXiv preprint arXiv:2401.11605*, 2024. 18

- Yaron Lipman, Ricky TQ Chen, Heli Ben-Hamu, Maximilian Nickel, and Matt Le. Flow matching for generative modeling. *arXiv preprint arXiv:2210.02747*, 2022. 19, 20
- Xingchao Liu, Chengyue Gong, and Qiang Liu. Flow straight and fast: Learning to generate and transfer data with rectified flow. *arXiv preprint arXiv:2209.03003*, 2022b. 19, 20
- Axel Sauer, Frederic Boesel, Tim Dockhorn, Andreas Blattmann, Patrick Esser, and Robin Rombach. Fast high-resolution image synthesis with latent adversarial diffusion distillation. *arXiv preprint arXiv:2403.12015*, 2024. 20
- Geoffrey E Hinton, Nitish Srivastava, Alex Krizhevsky, Ilya Sutskever, and Ruslan R Salakhutdinov. Improving neural networks by preventing co-adaptation of feature detectors. *arXiv preprint arXiv:1207.0580*, 2012. 20
- Andrew Brock, Jeff Donahue, and Karen Simonyan. Large scale gan training for high fidelity natural image synthesis. *arXiv preprint arXiv:1809.11096*, 2018. 22
- Tero Karras, Miika Aittala, Janne Hellsten, Samuli Laine, Jaakko Lehtinen, and Timo Aila. Training generative adversarial networks with limited data. In *Neural Information Processing Systems (NeurIPS)*, 2020. 22
- Axel Sauer, Katja Schwarz, and Andreas Geiger. Stylegan-xl: Scaling stylegan to large diverse datasets. In *ACM SIGGRAPH 2022 conference proceedings*, 2022. 22
- Yilun Xu, Ziming Liu, Yonglong Tian, Shangyuan Tong, Max Tegmark, and Tommi Jaakkola. Pfgm++: Unlocking the potential of physics-inspired generative models. In *International Conference on Machine Learning*, pages 38566–38591. PMLR, 2023b. 22
- Junlong Lyu, Zhitang Chen, and Shoubo Feng. Convergence guarantee for consistency models. *arXiv preprint arXiv:2308.11449*, 2023. 23
- Liyuan Liu, Haoming Jiang, Pengcheng He, Weizhu Chen, Xiaodong Liu, Jianfeng Gao, and Jiawei Han. On the variance of the adaptive learning rate and beyond. *arXiv preprint arXiv:1908.03265*, 2019. 25
- Diederik P Kingma and Jimmy Ba. Adam: A method for stochastic optimization. *arXiv preprint arXiv:1412.6980*, 2014. 25, 26
- Edward J Hu, Phillip Wallis, Zeyuan Allen-Zhu, Yanzhi Li, Shean Wang, Lu Wang, Weizhu Chen, et al. Lora: Low-rank adaptation of large language models. In *International Conference on Learning Representations*, 2021. 25

## A MOTIVATIONS BEHIND DESIGN CHOICES IN ECT

In this section, we expand upon our motivation behind the design decisions for the mapping function, metric, and weighting function used for ECT.

**Mapping Function.** We first assume that  $\Delta t$  is *approximately* proportional to  $t$ . Let  $0 < c \leq 1$  be this constant of proportionality, then we can write:

$$c \approx \frac{\Delta t}{t} = \frac{t - r}{t} = 1 - \frac{r}{t} \Rightarrow \frac{r}{t} \approx 1 - c.$$

As training progresses, the mapping function should gradually shrink  $\Delta t \rightarrow 0$ . However, the above parameterization does not achieve this. An alternative parameterization is to decrease  $\Delta t$  exponentially. We assume the ratio between  $r$  and  $t$  can be written as:

$$\frac{r}{t} = 1 - \frac{1}{q^a}, \quad (17)$$

where  $q > 1$ ,  $a = \lfloor \text{iters}/d \rfloor$ , and  $d$  is a hyperparameter controlling how quickly  $\Delta t \rightarrow dt$ . At the beginning of training,  $\frac{r}{t} = 1 - \frac{1}{q^0} = 0 \Rightarrow r = 0$ , which falls back to DMs. Since we can initialize from the diffusion pretraining, this stage can be skipped by setting  $a = \lceil \text{iters}/d \rceil$ . As training progresses ( $\text{iters} \uparrow$ ),  $\frac{r}{t} \rightarrow 1$  leads to  $\Delta t \rightarrow dt$ .

Finally, we adjust the mapping function to balance the prediction difficulties across different noise levels:

$$\frac{r}{t} = 1 - \frac{1}{q^a n(t)} = 1 - \frac{1}{q^{\lceil \text{iters}/d \rceil} n(t)}. \quad (18)$$

For  $n(t)$ , we choose  $n(t) = 1 + k, \sigma(-b, t) = 1 + \frac{k}{1 + e^{bt}}$ , using the sigmoid function  $\sigma$ . Since  $r \geq 0$ , we also clamp  $r$  to satisfy this constraint after the adjustment.

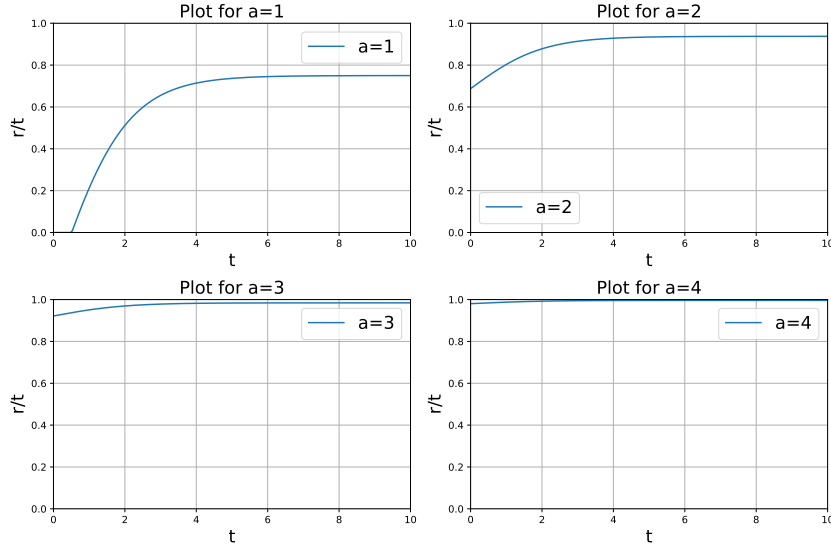


Figure 5: Visualization of  $r/t$  during training.  $\Delta t \rightarrow dt$  when  $r/t \rightarrow 1$ .

The intuition behind this mapping function is that the relative difficulty of predicting  $f(\mathbf{x}_r)$  from  $\mathbf{x}_t$  can vary significantly across different noise levels  $t$  when using a linear mapping between  $t$  and  $r$ .

Consider  $r/t = 0.9$ . At small values of  $t$ ,  $\mathbf{x}_t$  and  $\mathbf{x}_r$  are close, making the alignment of  $f(\mathbf{x}_t)$  with  $f(\mathbf{x}_r)$  relatively easy. In contrast, at larger  $t$ , where  $\mathbf{x}_t$  and  $\mathbf{x}_r$  are relatively far apart, the distance between the predictions  $f(\mathbf{x}_t)$  and  $f(\mathbf{x}_r)$  can be substantial. This leads to imbalanced gradient flows across different noise levels, impeding the training dynamics.

Therefore, we downscale  $r/t$  when  $t$  is near 0 through the mapping function, balancing the gradient flow across varying noise levels. This prevents the gradient at any noise level from being too small or too large relative to other noise levels, thereby controlling the variance of the gradients.

We direct the reader to Appendix B for details of how to set  $q^{\lceil \text{iters}/d \rceil}$ .

**Choice of Metric.** As discussed in Sec. 2, iCT uses pseudo-Huber metric (Charbonnier et al., 1997) to mitigate the perceptual bias caused by the LPIPS metric (Zhang et al., 2018),

$$L(\mathbf{x}, \mathbf{y}) = \sqrt{\|\mathbf{x} - \mathbf{y}\|_2^2 + \epsilon} - \epsilon, \quad \epsilon > 0. \quad (19)$$

This metric indeed improves the performance of CMs over the classic squared  $L_2$  loss. When taking a careful look at this metric, we reveal that one of the reasons for this improvement is that this metric is more robust to the outliers compared to the  $L_2$  metric due to its adaptive per-sample scaling of the gradients. Let  $\Delta = \mathbf{x} - \mathbf{y}$ , then the differential of the pseudo-Huber metric can be written as

$$dL = \underbrace{\frac{1}{\sqrt{\|\Delta\|_2^2 + c^2}}}_{\text{weighting term}} \underbrace{d\left(\frac{1}{2}\|\Delta\|_2^2\right)}_{\text{differential of squared } L_2 \text{ loss}}, \quad (20)$$

where we have decomposed the differential of pseudo-Huber loss into an adaptive weighting term and the differential of the squared  $L_2$  loss. Therefore, we retain the squared  $L_2$  metric used in DMs, and explore varying adaptive weighting terms which we explore in detail in Appendix B.

**Distinction between the training schedules of ECT and iCT.** As noted in Sec. 2, iCT (Song and Dhariwal, 2023) employs a discrete-time curriculum given by Eq. (8). This curriculum divides the noise horizon  $[0, T]$  into  $N$  smaller consecutive subintervals to apply the consistency loss, characterized by non-overlapping segments  $[t_i, t_{i+1}]$ , and gradually increases the number of intervals  $N = 10 \rightarrow 1280$ . However, the "boundary" condition of this schedule is to start with the number of intervals to  $N = 1$ , learning a model solely mapping samples at noise levels  $T_{\max}$  to the clean data  $\mathbf{x}_0$ , largely distinct from the classic diffusion models training. We instead investigate a continuous-time schedule whose "boundary" condition yields diffusion pretraining, *i.e.*, constructing training pairs of  $r = 0$  for all  $t$  at the beginning.

## B EXPLORING DESIGN SPACE & SCALING OF CONSISTENCY MODELS

Due to ECT’s efficiency, we can explore the design space of CMs at a minimal cost. We specifically examine the weighting function, training schedule, and regularization for CMs.

Our most significant finding is that *controlling gradient variances and balancing the gradients across different noise levels are fundamental to CMs’ training dynamics*. Leveraging the deep connection between CMs and DMs, we also improve the diffusion pretraining and the full pretraining+tuning pipeline using our findings.

**Weighting Function.** Forward processes with different noise schedules and model parameterizations can be translated into each other at the cost of varying weighting functions (Kingma and Gao, 2024). From our experiments on a wide range of weighting schemes, we learn three key lessons.

(1) *There is no free lunch for weighting function, i.e.*, there is likely no universal timestep weighting  $\bar{w}(t)$  that can outperform all other candidates on different datasets, models, and target metrics for both 1-step and 2-step generation.

We refer these results to Tab. 2, including  $\text{SNR}(t) = 1/t^2$ ,  $\text{SNR}(t) + 1 = 1/t^2 + 1$  (Salimans and Ho, 2022), EDM weighting  $\text{SNR}(t) + 1/\sigma_{\text{data}}^2 = 1/t^2 + 1/\sigma_{\text{data}}^2$  (Karras et al., 2022), and Soft-Min-SNR weighting  $1/(t^2 + \sigma_{\text{data}}^2)$  (Hang et al., 2023; Crowson et al., 2024), where  $\text{SNR}(t) = 1/t^2$  is the signal-to-noise ratio in our setup.

On CIFAR-10, the weighting  $\bar{w}(t) = 1/(t-r)$  from the discretization of consistency condition in Eq. (12) achieves the best 1-step FID, while the square root of  $\text{SNR}(t)$ ,  $\bar{w}(t) = \sqrt{\text{SNR}(t)} = 1/t$ , produces the best  $\text{FD}_{\text{DINOv2}}$ . On ImageNet  $64 \times 64$ , considering that we have already had the adaptive

Table 2: Performance of ECMs trained with various weighting functions on ImageNet  $64 \times 64$ . We enable the adaptive weighting  $w(\Delta) = 1/(\|\Delta\|_2^2 + c^2)^{\frac{1}{2}}$ .

$\bar{w}(t)$	1-step FID↓	2-step FID↓
1	<b>5.39</b>	3.48
$1/t$	17.79	3.24
$1/(t-r)$	9.28	3.22
$1/t + 1/\sigma_{\text{data}}$	5.68	3.44
$1/t^2$	190.80	20.65
$1/t^2 + 1$	6.78	<b>3.12</b>
$1/t^2 + 1/\sigma_{\text{data}}^2$	5.51	3.18
$1/(t^2 + \sigma_{\text{data}}^2)$	163.01	13.33

Table 3: Performance of ECMs trained with varying adaptive weightings on ImageNet  $64 \times 64$ .

$\bar{w}(t)$	$w(\Delta)$	1-step FID↓	2-step FID↓
$1/t^2 + 1/\sigma_{\text{data}}^2$	1	6.51	3.28
$1/t^2 + 1/\sigma_{\text{data}}^2$	$1/(\ \Delta\ _1 + c)$	6.29	3.25
$1/t^2 + 1/\sigma_{\text{data}}^2$	$1/(\ \Delta\ _2^2 + c^2)^{\frac{1}{2}}$	5.51	3.18
1	$1/(\ \Delta\ _2^2 + c^2)^{\frac{1}{2}}$	5.39	3.48

weighting  $w(\Delta)$ , the uniform weighting  $\bar{w}(t) \equiv 1$  can demonstrate the best 1-step FID when tuning from EDM2 (Karras et al., 2024). In contrast to 1-step FIDs, a wider range of timestep weighting  $\bar{w}(t)$  produces close 2-step FIDs for ECMs.

When starting on a new dataset with no prior information,  $\bar{w}(t) = \text{SNR}(t) + n$  is a generally strong choice as the default timestep weighting of data prediction models (x-pred). In this situation, this weighting function corresponds to using v-pred (Salimans and Ho, 2022) or flow matching (Lipman et al., 2022; Liu et al., 2022b) as model parameterization when  $n = 1$ .

(2) *The adaptive weighting  $w(\Delta)$  achieves better results by controlling gradient variance.* The adaptive weighting  $w(\Delta)$  on a per-sample basis shows uniform improvements on both CIFAR-10 and ImageNet  $64 \times 64$ . See Tab. 3 for the ablation study.

Beyond ECT, we further investigate the role of adaptive weighting  $w(\Delta)$  in pretraining on a toy Swiss roll dataset using the parameterization and forward process of flow matching (Lipman et al., 2022) and an MLP network.

Consider the objective function  $w(\Delta) \|v_\theta(\mathbf{x}_t) - (\mathbf{x}_1 - \mathbf{x}_0)\|_2^2$ , where  $\mathbf{x}_t = (1 - t) \cdot \mathbf{x}_0 + t \cdot \mathbf{x}_1$ ,  $t \sim \text{Uniform}(0, 1)$ ,  $\mathbf{x}_1 \sim \mathcal{N}(\mathbf{0}, \mathbf{I})$ , and the adaptive weighting

$$w(\Delta) = \frac{1}{(\|\Delta\|_2^2 + \epsilon)^p},$$

where  $p = 0$  corresponds to no adaptive weighting. We set  $\epsilon = 10^{-6}$  and control the strength of gradient normalization by varying  $p$  from 0 to 1.

As we increase the strength of adaptive weighting, flow models become easier to sample from in a few steps. Surprisingly, even  $p = 1$  demonstrates strong few-step sampling results when pretraining the flow model. See Fig. 6 for visualization.

**Mapping Function.** We compare the constant mapping function with  $n(t) \equiv 1$  in Eq. (17) and mapping function equipped with the sigmoid  $n(t)$  in Eq. (18). We use  $k = 8$  and  $b = 1$  for all the experiments, which transfers well from CIFAR-10 to ImageNet  $64 \times 64$  and serves as a baseline in our experiments. Though  $b = 2$  can further improve the 1-step FIDs on ImageNet  $64 \times 64$ , noticed post hoc, we don’t rerun our experiments.

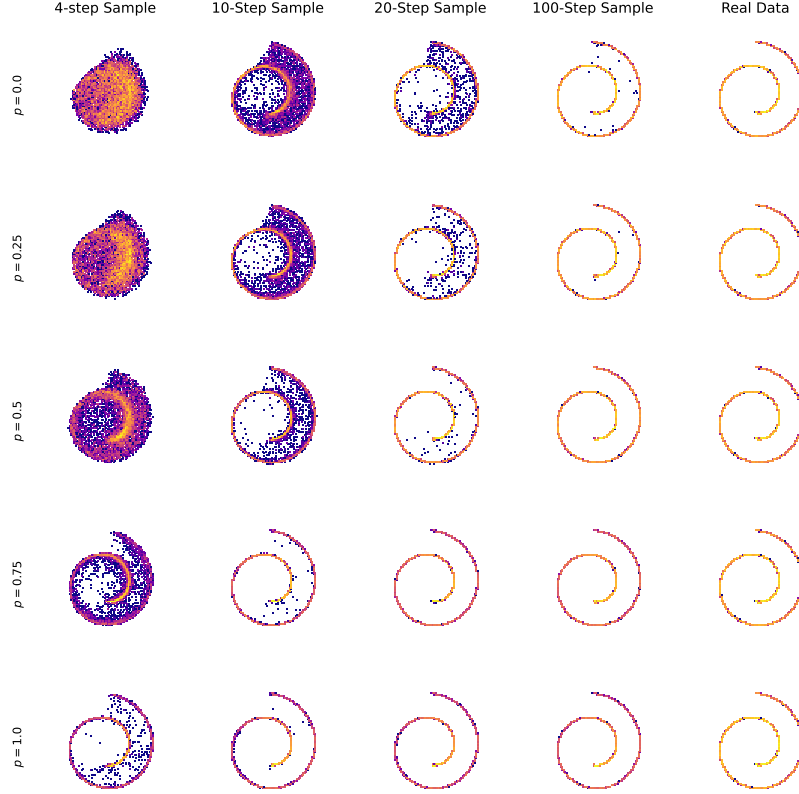


Figure 6: Influence of adaptive weighting  $w(\Delta) = 1/(\|\Delta\|_2^2 + \epsilon)^p$  on pretraining using varying  $p$ .

On CIFAR-10, the constant mapping function with  $n(t) \equiv 1$  achieves 1-step FID of 4.06 at 200k iterations, worse than the 1-step FID of 3.86 by  $n(t) = 1 + \frac{k}{1+e^{bt}}$ . Under our forward process ( $\mathbf{x}_t = \mathbf{x}_0 + t \cdot \epsilon$ ) and model parameterization (EDM (Karras et al., 2022)), the constant mapping function incurs training instability on ImageNet  $64 \times 64$ , likely due to the imbalanced gradient flow.

The role of the mapping function, regarding training, is to balance the difficulty of learning *consistency condition* across different noise levels, avoiding trivial consistency loss near  $t \rightarrow 0$ . For model parameterizations and forward processes different from ours, for example, flow matching (Lipman et al., 2022; Liu et al., 2022b; Sauer et al., 2024), we advise readers to start from the constant mapping function due to its simplicity.

**Dropout.** In line with (Song and Dhariwal, 2023), we find that CMs benefit significantly from dropout (Hinton et al., 2012). On CIFAR-10, we apply a dropout of 0.20 for models evaluated on FID and a dropout of 0.30 for models evaluated on  $\text{FD}_{\text{DINOv2}}$ .

On ImageNet  $64 \times 64$ , we note that ECM benefits from a surprisingly high dropout rate. When increasing the dropout rate from 0.10 to 0.40, the 2-step FID decreases from 4.53 to 3.24. Increasing the dropout rate further can be helpful for 1-step FID under certain timestep weighting  $\bar{w}(t)$ , but the 2-step FID starts to deteriorate. In general, we optimize our model configurations for 2-step generation and choose the dropout rate of 0.40 for ECM-S.

Finally, we note that the dropout rate tuned at a given weighting function  $w(t)$  transfers well to the other weighting functions, thereby reducing the overall cost of hyperparameter tuning. On ImageNet  $64 \times 64$ , the dropout rate can even transfer to different model sizes. We apply a dropout rate of 0.50 for all the model sizes of ECM-M/L/XL.

**Shrinking  $\Delta t \rightarrow dt$ .** In the mapping function discussed in Sec. 3.3 and Appendix A, we use the hyperparameter  $d$  to control the magnitude of  $q$ , thereby determining the overall rate of shrinking

$\Delta t \rightarrow dt$ , given by  $(1 - 1/q^{\lceil \text{iters}/d \rceil})$ . In practice, we set  $q = 2$  and  $d = \text{total\_iters}/8$  for CIFAR-10 experiments, and  $q = 4$  and  $d = \text{total\_iters}/4$  for ImageNet  $64 \times 64$  experiments, achieving  $r/t \approx 0.99$  at the end of training.

Compared with no shrinkage of  $\Delta t$ , where  $\Delta t \approx dt$  throughout, we find that shrinking  $\Delta t \rightarrow dt$  results in improved performance for ECMs. For example, on CIFAR-10, starting ECT directly with  $\Delta t \approx dt$  by setting  $q = 256$  (corresponding to  $r/t \approx 0.99$ ) leads to quick improvements in sample quality initially but slower convergence later on. The 1-step FID drops from 3.60 to 3.86 using the same 400k training iterations compared to gradually shrinking  $\Delta t \rightarrow dt$ . On ImageNet  $64 \times 64$ ,  $\Delta t \approx dt$  with  $q = 256$  from the beginning results in training divergence, as the gradient flow is highly imbalanced across noise levels, even when initializing from pretrained diffusion models.

This observation suggests that *ECT’s schedule should be adjusted according to the compute budget*. At small compute budgets, as long as training stability permits, directly approximating the *differential consistency condition* through a small  $\Delta t \approx dt$  leads to fast sample quality improvements. For normal to rich compute budgets, shrinking  $\Delta t \rightarrow dt$  generally improves the final sample quality, which is the recommended practice.

Using this feature of ECT, we demonstrate its efficiency by training ECMs to surpass previous Consistency Distillation, which took hundreds of GPU hours, using **one hour on a single A100 GPU**.

**Training Generative Models in 1 GPU Hour.** Deep generative models are typically computationally expensive to train. Unlike training a classifier on CIFAR-10, which usually completes within one GPU hour, leading generative models on CIFAR-10 as of 2024 require days to a week to train on 8 GPUs. Even distillation from pretrained diffusion models can take over a day on 8 GPUs or even more, equivalently hundreds of GPU hours.

To demonstrate the efficiency of ECT and facilitate future studies, we implemented a fast prototyping setting designed to yield results within one hour on a single GPU. This configuration uses a fixed  $\Delta t \approx dt$  by setting  $q = 256$  in our mapping function (corresponding to  $r/t \approx 0.99$ ), which allows for quick approximation of the differential consistency condition. Through 8000 gradient descent steps at batch size of 128, within 1 hour on a single A100 40GB GPU, ECT achieves a 2-step FID of 2.73, outperforming Consistency Distillation (2-step FID of 2.93) trained with 800k iters at batch size 512 and LPIPS (Zhang et al., 2018) metric.

**Ablation on Pretraining** We conducted a controlled experiment, training CMs from scratch following iCT best practices and tuning EDM using both iCT and ECT schedules. The combined pretraining and fine-tuning cost for ECT is 50% + 6.25% of iCT trained from scratch. Results are presented in Tab. 4.

There is a noticeable performance gap between iCT’s training and ECT’s pretraining+tuning scheme, particularly when evaluating models using modern metrics like  $\text{FD}_{\text{DINOv2}}$  (Stein et al., 2024).  $\text{FD}_{\text{DINOv2}}$  employs the representation space of the DINOv2-L model (Oquab et al., 2023) to compute distributional distance, which has been shown to better align with human evaluations.

Table 4: Impact of pretraining on model performance

Model	$\text{FD}_{\text{DINOv2}}$
iCT	242.30
Pretraining + iCT tuning	200.31
Pretraining + ECT tuning	190.13
EDM	168.16

When scaling up the pretraining+tuning cost to match the overall cost of iCT in class-conditional settings, ECM achieves a  $\text{FD}_{\text{DINOv2}}$  of 152.21, significantly outperforming the iCT model trained from scratch (205.11). For context, StyleGAN-XL achieves an  $\text{FD}_{\text{DINOv2}}$  of 204.60.

**Ablation on Tuning Design Choices** Besides quantitatively evaluating the pretraining impact, we conduct further ablation studies regarding fine-tuning design choices. Due to the computational constraints, we tune EDM2-S using iCT’s design choices as the baseline. Results are presented

Table 5: Generative performance on class-conditional CIFAR-10.

Method	FD <sub>DINOv2</sub> ↓	NFE↓
GANs		
BigGAN (Brock et al., 2018)	326.66	1
StyleGAN2-ADA (Karras et al., 2020)	305.92	1
StyleGAN-XL (Sauer et al., 2022)	204.60	1
Diffusion Models		
EDM (Karras et al., 2022)	145.20	35
PFGM++ (Xu et al., 2023b)	141.65	35
ECT		
ECM (ECT Pretrained)	121.05	35
ECM (Tuned)	198.51	1
ECM (Tuned)	128.63	2

in Tab. 6. These results demonstrate the improvements of the continuous-time training schedule, increased dropout, and weighting functions on ECMs’ generative performance.

Table 6: Ablation study of continuous-time CMs on ImageNet 64×64

Methods	1-step FID	2-step FID
iCT + EDM2 Pretraining	21.09	4.39
+ Continuous-time schedule	14.34	4.33
+ Dropout = 0.40	9.28	3.22
+ $\bar{w}(t) = 1/t^2 + 1/\sigma_{\text{data}}^2$	5.51	3.18

**Improving Pretraining using Findings in Tuning.** The exploration of the design space through the tuning stage as a proxy led to a question: Can the insights gained during tuning be applied to improve the pretraining stage and, consequently, the entire pretraining+tuning pipeline for CMs? The results of our experiments confirmed this hypothesis.

For the largest  $\Delta t = t$ , ECT falls back to diffusion pretraining with  $r = 0$  and thus  $f_\theta(\mathbf{x}_r) = \mathbf{x}_0$ . We pretrain EDM (Karras et al., 2022) on the CIFAR-10 dataset using the findings in ECT. Instead of using EDM weighting,  $\text{SNR}(t) + 1/\sigma_{\text{data}}^2$ , we enable the adaptive weighting  $w(\Delta)$  with  $p = 1/2$  and smoothing factor  $c = 0$  and a timestep weighting  $\bar{w}(t) = 1/t$ .

Compared with the EDM baseline, the recipe from ECT brings a convergence acceleration over  $2\times$  regarding FD<sub>DINOv2</sub>, matching EDM’s final performance using less than half of the pretraining budget and largely outperforming it at the full pretraining budget.

EDM pretrained by ECT achieves FD<sub>DINOv2</sub> of 150.39 for unconditional generation and 121.05 for class-conditional generation, considerably better than the EDM baseline’s FD<sub>DINOv2</sub> of 168.17 for unconditional generation and 145.20 for class-conditional generation, when using the same pretraining budget and inference steps (NFE=35).

**Influence of Pretraining Quality.** Using ECT pretrained models (FD<sub>DINOv2</sub> of 121.05) and original EDM (Karras et al., 2022) (FD<sub>DINOv2</sub> of 145.20), we investigate the influence of pretraining quality on consistency tuning and resulting ECMs. Our experiments confirm that better pretraining leads to easier consistency tuning and faster convergence. At the same budget of 204.8M images, tuning from ECT pretrained models achieves FD<sub>DINOv2</sub> of 128.63, better than FD<sub>DINOv2</sub> of 152.21 from EDM.

ECM from the ECT pretraining surpasses SoTA GANs in 1 sampling step and advanced DMs in 2 sampling steps, only slightly falling behind our pretrained models and setting up a new SoTA for the modern metric FD<sub>DINOv2</sub>. Results can be found in Tab. 5.

On ImageNet 64×64, ECM-M, initialized from EDM2-M (Karras et al., 2024), deviates from the power law scaling and achieves better generative performance than the log-linear trend. (See Fig. 4,

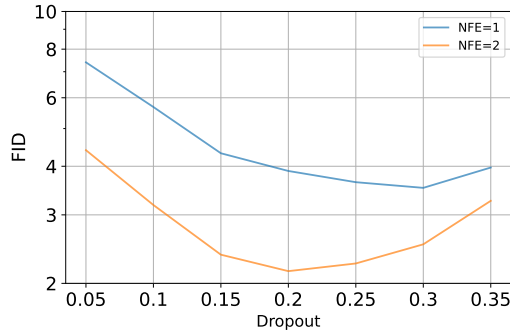


Figure 7: Relationship between the dropout and FIDs for models trained on CIFAR-10 with varying numbers of function evaluations (NFE) at inference.

Right). We speculate that it is due to a higher pretraining budget, in which EDM2-M was pretrained by  $2\times$  training images compared with other model sizes (S/L/XL).

**Differences between 1-step and 2-step Generation.** Our empirical results suggest that the training recipe for the best 1-step generative models can differ from the best few-step generative models in many aspects, including weighting function, dropout rate, and EMA rate/length. Fig. 7 shows an example of how FIDs from different numbers of function evaluations (NFEs) at inference vary with dropout rates.

In our setups, starting from a proper model size, the improvements from 2-step sampling seem larger than doubling the model size but keeping 1-step sampling. In the prior works, iCT (Song and Dhariwal, 2023) employs  $2\times$  deeper model, but the 1-step generative performance can be inferior to the 2-step results from ECT. This finding is consistent with recent theoretical analysis (Lyu et al., 2023), which indicates a tighter bound on the sample quality for the 2-step generation compared to the 1-step generation.

**Pareto Frontier & Scaling Law.** The Pareto Frontier reveals a seemingly power law scaling behavior. Training configurations not optimized for the current compute budget, *i.e.*, not on the Pareto Frontier, deviate from this scaling. Simply scaling up the training compute without adjusting other parameters may result in suboptimal performance. In our compute scaling experiments, we increased the batch size and enabled the smoothing factor  $c$  in the adaptive weighting to maintain this trend.

## C EXTENSION TO CONSISTENCY DISTILLATION.

**Continuous-time Consistency Distillation** Consistency Distillation (CD) (Song et al., 2023) uses a fixed discrete schedule derived from a specific sampler, such as the EDM sampler. This approach inherently limits  $\Delta t \rightarrow dt$ , therefore causing a non-trivial discretization error on approximating the differential consistency condition. Building upon ECT, we extend our continuous-time schedule to Consistency Distillation, which we term Easy Consistency Distillation (ECD).

On ImageNet  $64\times 64$ , we implement Consistency Distillation as the baseline using pretrained EDM2-S (Karras et al., 2024) with weighting functions, noise distribution, and dropout. The results, shown in Tab. 7, demonstrate that continuous-time distillation improves upon the standard CD approach.

Given well-pretrained DMs, ECD typically demonstrates a performance advantage over ECT at smaller batch sizes (e.g., 128), primarily due to the variance reduction in approximating the score function:

$$\nabla_{\mathbf{x}_t} \log p(\mathbf{x}_t) = \mathbb{E}[\nabla_{\mathbf{x}_t} \log p(\mathbf{x}_t|\mathbf{x}_0)|\mathbf{x}_t]$$

This advantage stems from the teacher models, which provide a variance-reduced estimate of the score function compared to the Monte Carlo estimation used in ECT. However, this gap tends to narrow as we scale up to larger model sizes. Scaling compensates for the limited training budget and variances, closing the gap between the two.

Table 7: Easy Consistency Distillation (ECD) on ImageNet 64×64 using the same budget of 12.8M training images (batch size 128 and 100k iterations) as ECT in Tab. 1.

Methods	1-step FID	2-step FID
CD-S	8.18	3.71
ECD-S	3.33	2.10
ECD-M	2.78	1.92
ECD-XL	2.54	1.77

Consequently, while ECD may outperform ECT in resource-constrained scenarios or with smaller models, the distinction becomes less pronounced as we move to larger scales. This observation underscores the scaling factor (computational resources and model size) when choosing between ECT and ECD for a given application.

**Data-Free ECD.** Inspired by the recent progress on data-free distillation (Luo et al., 2024; Gu et al., 2023; Yin et al., 2023; Zhou et al., 2024a), we explore a data-free variant of Easy Consistency Distillation (ECD). Instead of sampling data points  $\mathbf{x}_0$  from a given dataset  $\mathcal{D}$ , we generate synthetic data points directly from the CM itself on the fly,  $\mathbf{x}_0 = f_{\text{sg}(\theta)}(\epsilon', T)$ , where  $\epsilon' \sim p(\epsilon)$ ,  $T$  is the maximum noise level for sampling, followed by the same ECD training step over the self synthetic data. This eliminates the need for a distillation dataset or the construction of synthetic data from the teacher model (Luhman and Luhman, 2021; Geng et al., 2024; Zheng et al., 2023).

On ImageNet 64×64, this data-free ECD achieves 1-step FID of 4.38 and 2-step FID of 2.77, comparable to the data-dependent ECD and ECT schemes at the same budget. It suggests that data-free ECD can be a competitive alternative in scenarios where access to large datasets is limited or unavailable. We summarize both ECD and its data-free variant in Alg. 2.

---

**Algorithm 2** Easy Consistency Distillation (ECD) / Data-Free ECD

---

**Input:** Dataset  $\mathcal{D}$  (for ECD), a pretrained diffusion model  $\phi$ , mapping function  $p(r \mid t, \text{Iters})$ , weighting function  $w(t)$ .

**Init:**  $\theta \leftarrow \phi$ , Iters = 0.

**repeat**

**if** ECD **then**

    Sample  $\mathbf{x}_0 \sim \mathcal{D}$

**else if** Data-Free ECD **then**

    Sample  $\epsilon' \sim p(\epsilon)$

    Compute  $\mathbf{x}_0 = f_{\text{sg}(\theta)}(\epsilon', T)$

▷ sg is stop-gradient operator

**end if**

  Sample  $\epsilon \sim p(\epsilon)$ ,  $t \sim p(t)$ ,  $r \sim p(r \mid t, \text{Iters})$

  Compute  $\mathbf{x}_t = \mathbf{x}_0 + t \cdot \epsilon$ ,  $\Delta t = t - r$

  Compute  $\mathbf{x}_r = \text{Solver}(\mathbf{x}_t, t \rightarrow r, f_\phi)$

$L(\theta) = w(t) \cdot \mathbf{d}(f_\theta(\mathbf{x}_t), f_{\text{sg}(\theta)}(\mathbf{x}_r))$

$\theta \leftarrow \theta - \eta \nabla_\theta L(\theta)$

  Iters = Iters + 1

**until**  $\Delta t \rightarrow dt$  **return**  $\theta$

▷ ECD

---

## D EXPERIMENTAL DETAILS

**Model Setup.** For both unconditional and class-conditional CIFAR-10 experiments, we initial ECMs from the pretrained EDM (Karras et al., 2022) of DDPM++ architecture (Song et al., 2021b). For class-conditional ImageNet 64×64 experiments, we initial ECM-S/M/L/XL, ranging from 280M to 1.1B, from the pretrained EDM2 (Karras et al., 2024). Detailed model configurations are presented in Tab. 8.

We follow (Karras et al., 2022; Song et al., 2023) and set  $c_{\text{skip}}(t) = \sigma_{\text{data}}^2 / (t^2 + \sigma_{\text{data}}^2)$  and  $c_{\text{out}}(t) = t\sigma_{\text{data}} / \sqrt{t^2 + \sigma_{\text{data}}^2}$ , where  $\sigma_{\text{data}}^2$  is the variance of (normalized) data, and set to 0.5 for both CIFAR-10 and ImageNet 64×64.

Table 8: Model Configurations and Training Details for unconditional and class-conditional ECMs on CIFAR-10, and ECM-S/M/L/XL on ImageNet 64×64.

Model Setups	Uncond CIFAR-10	Cls-Cond CIFAR-10	ImageNet 64×64			
			ECM-S	ECM-M	ECM-L	ECM-XL
Model Channels	128	128	192	256	320	384
Model capacity (Mparams)	55.7	55.7	280.2	497.8	777.5	1119.3
Model complexity (GFLOPs)	21.3	21.3	101.9	180.8	282.2	405.9
<b>Training Details</b>						
Training Duration (Mimg)	12.8	12.8	12.8	12.8	12.8	12.8
Minibatch size	128	128	128	128	128	128
Iterations	100k	100k	100k	100k	100k	100k
Dropout probability	20%	20%	40%	50%	50%	50%
Dropout feature resolution	-	-	$\leq 16 \times 16$	$\leq 16 \times 16$	$\leq 16 \times 16$	$\leq 16 \times 16$
Optimizer	RAdam	RAdam	Adam	Adam	Adam	Adam
Learning rate max ( $\alpha_{\text{ref}}$ )	0.0001	0.0001	0.0010	0.0009	0.0008	0.0007
Learning rate decay ( $t_{\text{ref}}$ )	-	-	2000	2000	2000	2000
EMA beta	0.9999	0.9999	-	-	-	-
<b>Training Cost</b>						
Number of GPUs	1	1	4	8	8	8
GPU types	A6000	A6000	H100	H100	H100	H100
Training time (hours)	24	24	8.5	8.5	12	15
<b>Generative Performance</b>						
1-step FID	4.54	3.81	5.51	3.67	3.55	3.35
2-step FID	2.20	2.02	3.18	2.35	2.14	1.96
<b>ECT Details</b>						
Regular Weighting ( $\bar{w}(t)$ )	$1/(t-r)$	$1/(t-r)$	$1/t^2 + 1/\sigma_{\text{data}}^2$	$1/t^2 + 1/\sigma_{\text{data}}^2$	$1/t^2 + 1/\sigma_{\text{data}}^2$	$1/t^2 + 1/\sigma_{\text{data}}^2$
Adaptive Weighting ( $w(\Delta)$ )	✓	✓	✓	✓	✓	✓
Adaptive Weighting Smoothing ( $c$ )	0.0	0.0	0.06	0.06	0.06	0.06
Noise distribution mean ( $P_{\text{mean}}$ )	-1.1	-1.1	-0.8	-0.8	-0.8	-0.8
Noise distribution std ( $P_{\text{std}}$ )	2.0	2.0	1.6	1.6	1.6	1.6

**Computational Cost.** ECT is computationally efficient. On ImageNet 64×64, the tuning stage of ECT requiring only 0.39% of the iCT (Song and Dhariwal, 2023) training budget, and 0.60% to 1.91% of the EDM2 (Karras et al., 2024) pretraining budget depending on the model sizes. The exact computational resources required to train each individual model are shown in Tab. 8.

**Training Details.** We use RAdam (Liu et al., 2019) optimizer for experiments on CIFAR-10 and Adam (Kingma and Ba, 2014) optimizer for experiments on ImageNet 64×64. We set the  $\beta$  to (0.9, 0.999) for CIFAR-10 and (0.9, 0.99) for ImageNet 64×64. All the hyperparameters are indicated in Tab. 8. We do not use any learning rate decay, weight decay, or warmup on CIFAR-10. We follow EDM2 (Karras et al., 2024) to apply an inverse square root learning rate decay schedule on ImageNet 64×64.

On CIFAR-10, we employ the traditional Exponential Moving Average (EMA). To better understand the influence of the EMA rate, we track three Power function EMA (Karras et al., 2024) models on ImageNet 64×64, using EMA lengths of 0.01, 0.05, and 0.10. The multiple EMA models introduce no visible cost to the training speed. Considering our training budget is much smaller than the diffusion pretraining stage, we didn’t perform Post-Hoc EMA search as in EDM2 (Karras et al., 2024).

Experiments for ECT are organized in a non-adversarial setup to better focus and understand CMs and avoid inflated FID (Stein et al., 2024). We conducted ECT using full parameter tuning in this work, even for models over 1B parameters. Investigating the potential of Parameter Efficient Fine Tuning (PEFT) (Hu et al., 2021) can further reduce the cost of ECT to democratize efficient generative models, which is left for future research.

We train multiple ECMs with different choices of batch sizes and training iterations. By default, experiments on ImageNet 64×64 utilize a batch size of 128 and 100k iterations, leading to a training budget of 12.8M. We have individually indicated other training budgets alongside the relevant experiments, wherever applicable.

**Sampling Details.** We apply stochastic sampling for 2-step generation. For 2-step sampling, we follow (Song and Dhariwal, 2023) and set the intermediate  $t = 0.821$  for CIFAR-10, and  $t = 1.526$  for ImageNet  $64 \times 64$ .

Intriguingly, these sampling schedules, originally developed for iCT, also perform well with our ECMs. This effectiveness across different CMs and training methods likely links to the inherent characteristics of the datasets and the forward process. Developing a scientific approach to determine optimal intermediate sampling schedules for CMs remains an open research problem.

**Evaluation Metrics.** For both CIFAR-10 and ImageNet  $64 \times 64$ , FID and  $\text{FD}_{\text{DINOv2}}$  are computed using 50k images sampled from ECMs. As suggested by recent works (Stein et al., 2024; Karras et al., 2024),  $\text{FD}_{\text{DINOv2}}$  aligns better with human evaluation. We use `dgm-eval`<sup>1</sup> to calculate  $\text{FD}_{\text{DINOv2}}$  (Stein et al., 2024) to ensure align with previous practice.

**Visualization Setups.** Image samples in Fig. 3 are from class bubble (971), class flamingo (130), class golden retriever (207), class space shuttle (812), class Siberian husky (250), class ice cream (928), class oscilloscope (688), class llama (355), class tiger shark (3).

Each triplet (left-to-right) includes from 2-step samples from ECM-S trained with 12.8M images, ECM-S trained with 102.4M images, and ECM-XL trained with 102.4M images.

**1 GPU Hour Prototyping Settings.** This configuration uses a fixed  $\Delta t \approx dt$  by setting  $q = 256$  in our mapping function (corresponding to  $\frac{r}{t} \approx 0.99$ ) and an EMA rate of 0.9993 for the model parameters. Using these settings, we run 8000 gradient descent steps with a batch size of 128 on a single A100 40GB GPU.

**Scaling of Training Compute.** For the results on scaling laws for training compute on CIFAR-10 shown in Fig. 4 (Left), we train 6 class-conditional ECMs, each with varying batch size and number of training iterations. All ECMs in this experiment are initialized from the pretrained class-conditional EDM.

The minimal training compute at  $2^0$  scale corresponds to a total budget of 12.8M training images. The largest training compute at  $2^5$  scale utilizes a total budget of 409.6M training images, at  $2 \times$  EDM pretraining budget.

The first two points of  $2^0$  and  $2^1$  on Fig. 4 (Left) use a batch size of 128 for 100k and 200k iterations, respectively. The third point of  $2^2$  corresponds to ECM trained with batch sizes of 256 for 200k iterations. The final three points of  $2^3$ ,  $2^4$ , and  $2^5$  correspond to ECM trained with a batch size of 512 for 200k, 400k, and 800k iterations, respectively, with the smoothing factor  $c = 0.03$  enabled in the adaptive weighting  $w(\Delta)$ . We use  $\bar{w}(t) = 1/t$  as the timestep weighting function to train all these models as this  $\bar{w}(t)$  achieves good performance on  $\text{FD}_{\text{DINOv2}}$ .

**Scaling of Model Size and Model FLOPs.** We include details of model capacity as well as FLOPs in Tab. 8 to replicate this plot on ImageNet  $64 \times 64$ .

On ImageNet  $64 \times 64$ , we scale up the training budgets of ECM-S and ECM-XL from 12.8M (batch size of 128 and 100k iterations) to 102.4M (batch size of 1024 and 100k iterations). We empirically find that scaling the base learning rate by  $\sqrt{n}$  works well when scaling the batch size by a factor of  $n$  when using Adam (Kingma and Ba, 2014) optimizer.

## E QUALITATIVE RESULTS

We provide some randomly generated 2-step samples from ECMs trained on CIFAR-10 and ImageNet- $64 \times 64$  in Fig. 8 and Fig. 9, respectively.

<sup>1</sup><https://github.com/layer6ai-labs/dgm-eval>



Figure 8: 2-step samples from class-conditional ECM trained on CIFAR-10. Each row corresponds to a different class.

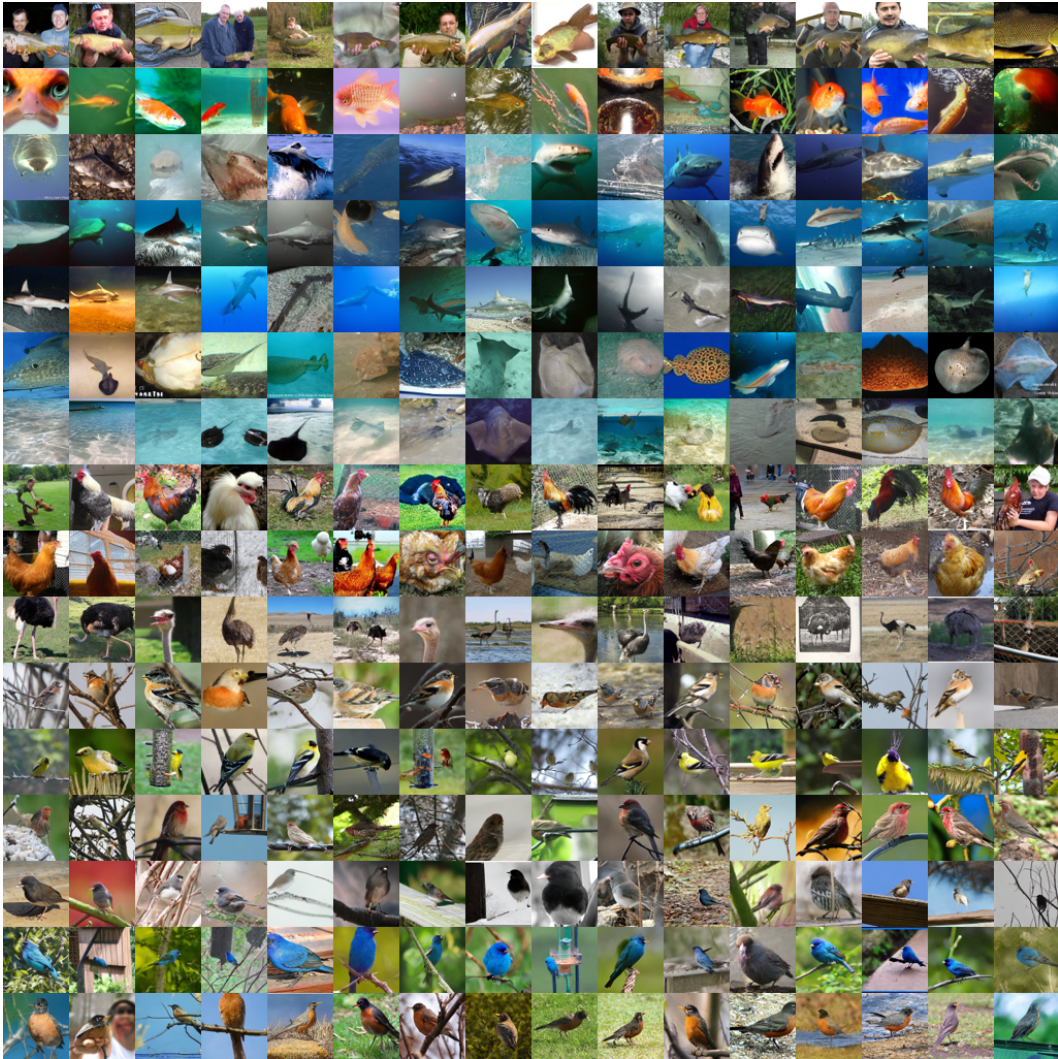


Figure 9: 2-step samples from class-conditional ECM-XL trained on ImageNet  $64 \times 64$ . Each row corresponds to a different class.